
SPDE PRIORS FOR UNCERTAINTY QUANTIFICATION OF END-TO-END NEURAL DATA ASSIMILATION SCHEMES

Maxime Beauchamp
IMT Atlantique
maxime.beauchamp@imt-atlantique.fr

Ronan Fablet
IMT Atlantique
ronan.fablet@imt-atlantique.fr

J. Emmanuel Johnson
IGE Grenoble
johnsonj@univ-grenoble-alpes.fr

Simon Benaïchouche
IMT Atlantique
simon.benaichouche@imt-atlantique.fr

Pierre Tandoe
IMT Atlantique
pierre.tandoe@imt-atlantique.fr

Nicolas Desassis
Mines ParisTech
nicolas.desassis@mines-paristech.fr

February 6, 2024

Abstract

The spatio-temporal interpolation of large geophysical datasets has historically been addressed by Optimal Interpolation (OI) and more sophisticated equation-based or data-driven data assimilation (DA) techniques. In the last ten years, the link established between Stochastic Partial Differential Equations (SPDE) and Gaussian Markov Random Fields (GMRF) opened a new way of handling both large datasets and physically-induced covariance matrix in Optimal Interpolation. Recent advances in the deep learning community also enables to adress this problem as neural architecture embedding data assimilation variational framework. The reconstruction task is seen as a joint learning problem of the prior involved in the variational inner cost, seen here as a projection operator of the state, and the gradient-based minimization of the latter: both prior models and solvers are stated as neural networks with automatic differentiation which can be trained by minimizing a loss function, typically stated as the mean squared error between some ground truth and the reconstruction. Such a strategy turns out to be very efficient to improve the mean state estimation, but still needs complementary developments to quantify its related uncertainty. In this work, we draw from the SPDE-based Gaussian Processes to estimate complex prior models able to handle non-stationary covariances in both space and time and provide a stochastic framework for interpretability and uncertainty quantification. Our neural variational scheme is modified to embed an augmented state formulation with both state and SPDE parametrization to estimate. Again, the problem is addressed as a joint learning problem but instead of a neural prior, we use a stochastic PDE as surrogate model along the data assimilation window. The training involves a loss function for both reconstruction task and SPDE prior model, where the likelihood of the SPDE parameters given the true states is involved in the training. Because the prior is stochastic, we can easily draw samples in the prior distribution before conditioning these by the neural scheme: the latter being fast, this provides a flexible way to estimate the posterior distribution based on thousands of members. We demonstrate the potential of the proposed framework on a spatio-temporal Gaussian Process driven by diffusion-based anisotropies and on realistic Sea Surface Height datasets. We show how our solution reaches the Optimal Interpolation baseline in the Gaussian case and how it outperforms the OI for non-linear dynamics while allowing for fast and interpretable online parameter estimation.

1 Introduction

Over the last decade, the emergence of large spatio-temporal datasets both coming from remote sensing satellites and equation-based numerical simulations has been noticed in Geosciences. As a consequence, the need for statistical methods able to handle both the size and the underlying physics of these data is growing. Data assimilation (DA) is the traditional framework used by geoscientists to merge these two types of information, data and model, by propagating information from observational data to areas with missing data. Broadly speaking, two main categories of DA [Evensen, 2009, Evensen et al., 2022] exists: variational and sequential methods. They both aims at minimizing some energy or functional involving a equation-based dynamical prior and an observation term. When no deterministic numerical outputs are available, the classic approach stems from the family of the so-called Optimal Interpolation (OI) techniques, see e.g. Traon et al. [1998]. OI is also known as (Simple) Kriging in Spatial Statistics [Chilès and Delfiner, 2012, Chilès and Desassis, 2018] and it directly relates to BLUE in the data assimilation formulation [Asch et al., 2016], being at the core of the statistical DA methods. The optimal interpolation implies to factorize dense covariance matrices which turns out to be an issue when the size of spatio-temporal datasets is large. Reduced rank approximations, see e.g. [Cressie and Wikle, 2015] have already been investigated to tackle this specific problem. More recently, the use of sparse precision matrices has also been proposed by using tapering strategies [Furrer et al., 2006, Bolin and Wallin, 2016] or by making use of the link seen by Lindgren et al. [2011] between Stochastic Partial Differential Equations (SPDE) and Gaussian Processes. For the latter, if the original link was made through the Poisson SPDE equation [Whittle, 1953], it can be extended to more complex linear SPDE involving physical processes like advection or diffusion [Lindgren et al., 2011, Fuglstad et al., 2015a, Clarotto et al., 2022]. Thus, it opens new avenue to cope with massive observational datasets in geosciences while making use of the underlying physics of such processes. Let note that the so-called SPDE-based approach can also be used as a general spatio-temporal model, even if it is not physically motivated, since it provides a flexible way to handle local anisotropies of a large set of geophysical processes. It has known numerous applications in the past few years, see e.g. Sigrist et al. [2015], Fuglstad et al. [2015b]. Though, when considering a spatio-temporal advection-diffusion SPDE, the parameters generally vary continuously across space and/or time making their estimation an additional problem to the original interpolation task. This estimation generally relies on off-line strategies [Fuglstad et al., 2015b] embedded in hierarchical models, which can be another computational issue while the set of parameters estimated does not automatically transfer to a new dataset.

From another point of view, deep learning frameworks are currently knowing an intense period of scientific contribution to revisit statistical methods with neural network formulation. The latter enables to use automatic differentiation embedded in the gradient-based optimization as a way of solving traditional inverse problems. In particular, when the problem relates to space-time interpolation of partial and noisy observation of geophysical fields, deep learning-based solutions has been recently proposed to jointly learn prior models and solvers as an end-to-end data-driven variational data assimilation scheme. In Fablet et al. [2020], the so-called 4DVarNet neural scheme is introduced: it involves an implicit iterative gradient-based LSTM solver to minimize a variational cost, close to what is encountered in 4DVar data assimilation [Carrassi et al., 2018]. In this variational cost, the dynamical prior is no longer equation-based but is stated as a trainable neural network learnt during the training process. Then, automatic differentiation is used to compute the gradient of the variational cost during the gradient-based iterations, instead of requiring the computation of complex and costly adjoint models [Asch et al., 2016]. Drawing from this framework, a neural optimal interpolation scheme has also been proposed [Beauchamp et al., 2022] to reach OI performance with a linear scaling of the solution on the number of space-time variables, leading to a significant speed up in the computation of the solution.

In this work, we draw from this last strategy to build a neural variational scheme that will jointly learn the solver and the SPDE parametrization as surrogate prior model for the evolution equation. Because the parameters of the SPDE remain initially unknown, they are embedded in the optimization process using an augmented state formulation, commonly used in data assimilation, see e.g. [Ruiz et al., 2013]. The solver is still based on an iterative residual scheme to update the analysis state. Here, the analysis stands for the expectation of the state given the observations, together with the SPDE parametrization maximizing their likelihood given the true states used during the training. The SPDE equation can then be seen as a tangent linear model of the prior along the data assimilation window, from which we provide uncertainty quantification throughout its precision matrix. Using such a stochastic prior entails the possibility of generating huge members in the posterior pdf, after conditioning of the prior samples by our neural

variational scheme. Also, if the training dataset is large enough, the method provides an efficient way to estimate *online* the SPDE parametrization for any new sequence of input observations, without any additional inference to make. In the end, the key contributions of this work are four-fold:

- We develop the explicit solver of the considered SPDE prior. It relies on the analytical expression for the SPDE-based precision matrix of any state trajectory, based on a finite-difference discretization of the grid covered by the tensors involved in our neural scheme;
- We exploit this SPDE parametrization as surrogate prior model in the proposed variational formulation and leverage a trainable gradient-based solver to address jointly the interpolation of the state trajectory and the estimation of SPDE parameters from irregularly-sampled observations. The end-to-end training of the solver targets both the expectation of the state given the observations, together with the SPDE parametrization maximizing its likelihood given the true states;
- The SPDE prior paves the way to uncertainty quantification through the sampling of the prior pdf and the conditioning by the neural gradient-based solver;
- We demonstrate how the proposed framework relates to many ideas commonly shared among generative deep learning models;

To present these contributions, the paper is structured as follows. In Section 2, we provide a preliminary background on spatial SPDE to explain how the use of sparse precision matrix leads to an efficient optimal interpolation scheme, which will be a key aspect in our use of the SPDE as prior model. In Section 3, we explain how to use SPDE-based prior as a surrogate model for the evolution equation, and detail the spatio-temporal extension of the spatial SPDE framework for both simulation and interpolation. We also explain how to handle the case of noisy observations in this setup, which will bring us back to a familiar state space data assimilation formalism. In Section 4, we start by describing how the SPDE parameters are the key to handle complex covariance structure in OI-based techniques. Then, we explain in Section 5 the proposed neural architecture: first, we present the neural variational scheme and how it transfers to OI scheme by making the explicit link between the general prior regularization term in the variational cost and the same using as prior a Gaussian Process. Based on this link, we present how to augment the state with the SPDE prior parametrization, how to plug such a prior in the neural iterative gradient-based scheme to bypass the computational inversion of large datasets, and finally how to choose the training loss function to optimize the latter. In Section 6, we mention some related works we believe important so that connection can be made in the different communities of Gaussian Processes, generative modeling and data assimilation. Finally in Section 7, we present two applications. First, we simulate a GP driven by a spatio-temporal SPDE with spatially varying diffusion parameters and assess how the proposed framework behaves in comparison with the optimal solution. Second, an application to Sea Surface Height realistic datasets is considered using an Observation System Simulation Experiment (OSSE) where the Ground Truth is provided by the numerical outputs of the state-of-the-art NEMO model in its NATL60 high resolution basin-scale configuration Molines [2018]. We compare our method to the DUACS operational baseline and demonstrates how the proposed framework is also relevant for non-gaussian and non-linear dynamics.

2 Background: SPDE-based simulations and interpolations: the spatial case

Most of Optimal Interpolation and kriging techniques applied to Gaussian Processes suffer from severe limitations when considering high dimensional systems. Indeed, OI requires to solve a linear system and the inversion of dense $p \times p$ covariance matrices comes with a computational cost of $\mathcal{O}(p^3)$, where p denotes the number of observations. From now on, we use notations from classic DA formulation. Typically the discretization of the GP $X(\mathbf{s})$, $\mathbf{s} \in \mathbb{R}^d$, ($d = 2$ in case of 2-dimensional fields), denotes \mathbf{x} , is called state space and lies in \mathbb{R}^m while the partial (and potentially noisy) observation dataset \mathbf{y} is in \mathbb{R}^p . The SPDE-based estimation model proposed by Lindgren et al. [2011] opens a new path to deal with large datasets by making use of sparse precision matrices to solve the linear system. It is constrained by the use of Matérn covariance model, see e.g. [Genton, 2002]:

$$C(\mathbf{h}) = \sigma^2 \frac{2^{1-\nu}}{\Gamma(\nu)} \left(\sqrt{2\nu} \frac{h}{a} \right)^\nu \mathcal{K}_\nu \left(\sqrt{2\nu} \frac{h}{a} \right)$$

where $h = |\mathbf{s} - \mathbf{s}'|$ denotes the distance between two spatial locations, Γ denotes the Gamma function, \mathcal{K}_ν is the modified 2nd order Bessel function, and ν is the parameter that controls the regularity of the covariance. Regarding the latter, the Matérn model is very general and allows for flexible covariance structure: let

note that for $\nu = 1/2$, we get the exponential covariance and for the limit $\nu \rightarrow +\infty$, we get the gaussian covariance for a suitable reparametrization of a .

If X is a Gaussian Process with Matérn covariance having regularity parameters ν , scale parameter a and variance σ^2 , then it is solution of the following SPDE [Whittle, 1953]:

$$(\kappa^2 - \Delta)^{\alpha/2} X = \tau Z \quad (1)$$

where $\Delta = \sum_{i=1}^d \frac{\partial^2}{\partial s_i^2}$ denotes the Laplacian operator, Z is a standard Gaussian white noise, $\kappa = 1/a$, $\alpha = \nu + d/2$ and τ is defined by:

$$\tau = \frac{\sigma \Gamma(\nu + d/2)^{1/2} (4\pi)^{d/4} \kappa^\nu}{\Gamma(\nu)^{1/2}} \quad (2)$$

where Γ denotes the Gamma function.

2.1 Simulation

Let now consider the state space $\mathbf{x} \in \mathbb{R}^m$ being the discretization of the continuous GP $X(\mathbf{s})$ on a regular grid (x_i, y_j) where $x_i = i\Delta x$, $i \in 1, \dots, N_x$ and $y_j = j\Delta y$, $j \in 1, \dots, N_y$. As a consequence, the k^{th} element of \mathbf{x} can be located either by its coordinates (x_k, y_k) or by indices (i, j) where $i = \lfloor k/N_x \rfloor$ and $j = k \bmod N_x$.

Using a finite difference method (FDM) applied on the Laplacian operator, we approach the partial derivative of X w.r.t coordinate y by a centered difference:

$$\frac{\partial X}{\partial y} = \frac{X(y + dy) - X(y - dy)}{2dy} \quad (3)$$

The same applies for the derivative w.r.t coordinate x . Then, the FDM discretization of the SPDE writes:

$$\kappa^2 \mathbf{x}_{i,j} - \frac{\mathbf{x}_{i-1,j} - 2\mathbf{x}_{i,j} + \mathbf{x}_{i+1,j}}{dx^2} - \frac{\mathbf{x}_{i,j-1} - 2\mathbf{x}_{i,j} + \mathbf{x}_{i,j+1}}{dy^2} = \tau \mathbf{z}_{i,j} \quad (4)$$

Using matrix notations, it leads to the linear system $\mathbf{B}\mathbf{x} = \tau\mathbf{z}$, where $\mathbf{B} = \mathbf{A}^{\alpha/2}$ (only the case where $\alpha/2 \in \mathbb{N}$ is considered here, for more general case, see e.g. Lindgren et al. [2011]) and matrix $\mathbf{A} = (A_{k,l})$ is the discretized version of the fractional differential operator $(\kappa^2 - \Delta)$:

$$\mathbf{A}_{k,l} = \begin{cases} -1/dx^2 & \text{if } l = k + 1 \text{ or } l = k - 1 \\ -1/dy^2 & \text{if } l = k + N_x \text{ or } l = k - N_x \\ \kappa^2 + 2(1/dx^2 + 1/dy^2) & \text{if } l = k \\ 0 & \text{otherwise} \end{cases} \quad (5)$$

$\mathbf{z} \in \mathbb{R}^m$ denotes the white noise vector discretized on the regular grid related to the state space \mathbf{x} . We can show that the discretization matrix \mathbf{A} of the differential operator is invertible [Rue and Held, 2005]. Regarding the precision matrix \mathbf{Q} of \mathbf{x} , i.e. the inverse of its covariance matrix \mathbf{P} , it writes:

$$\text{Cov}\{\mathbf{B}\mathbf{x}, \mathbf{B}\mathbf{x}\} = \mathbf{B}\mathbf{P}\mathbf{B}^\top = \tau^2 \text{Cov}\{\mathbf{z}, \mathbf{z}\} = \frac{\tau^2}{dxdy} \mathbf{I} \quad (6)$$

Then,

$$\mathbf{P} = \frac{\tau^2}{dxdy} (\mathbf{B})^{-1} (\mathbf{B}^\top)^{-1} \quad (7)$$

$$\mathbf{Q} = \mathbf{P}^{-1} = \frac{dxdy}{\tau^2} \mathbf{B}^\top \mathbf{B} \quad (8)$$

A non-conditional simulation of state \mathbf{x} is easily obtained by solving the linear system introduced above for a random Gaussian vector \mathbf{z} with independant components and variance τ/\sqrt{dxdy} .

2.2 Optimal Interpolation

Regarding Optimal Interpolation, the covariance matrix of $[\mathbf{y} \ \mathbf{x}]^T$ is:

$$\mathbf{P} = \begin{bmatrix} \mathbf{P}_{yy} & \mathbf{P}_{yx} \\ \mathbf{P}_{xy} & \mathbf{P}_{xx} \end{bmatrix} \quad (9)$$

with $\mathbf{P}_{yx}^T = \mathbf{P}_{xy}$

The OI or simple kriging (with zero mean) of \mathbf{x} is given by, see e.g. [Chilès and Delfiner, 2012]:

$$\mathbf{x}^* = \mathbf{P}_{xy}\mathbf{P}_{yy}^{-1}\mathbf{y} \quad (10)$$

where \mathbf{x}^* denotes the optimal estimation of state \mathbf{x} given the observations \mathbf{y} . Its error covariance matrix is:

$$\text{Cov}(\mathbf{x}^* - \mathbf{x}) = \mathbf{P}_{xx} - \mathbf{P}_{xy}\mathbf{P}_{yy}^{-1}\mathbf{P}_{yx}$$

This formula can be rewritten under precision-based formulation

$$\mathbf{x}^* = -\mathbf{Q}_{xx}^{-1}\mathbf{Q}_{xy}\mathbf{y} \quad (11)$$

with error covariance matrix:

$$\text{Cov}(\mathbf{x}^* - \mathbf{x}) = \mathbf{Q}_{xx}^{-1}$$

By construction, \mathbf{Q} is sparse and Eq.11 is solved using Cholesky decomposition $\mathbf{Q}_{xx} = \mathbf{L}\mathbf{L}^T$:

$$\mathbf{L}^T\mathbf{x}^* = -\mathbf{L}^{-1}\mathbf{Q}_{xy}\mathbf{y}$$

Let note that in the covariance-based setup, we invert a dense covariance matrix \mathbf{P}_{yy} which has size $p \times p$ while in the SPDE approach, we solve a system with sparse precision matrix \mathbf{Q}_{xx} of size generally equals to $m \times m$. In the latter, we use sparse matrices algorithm of complexity $\mathcal{O}(n^{3/2})$, while the general Cholesky algorithm is of complexity $\mathcal{O}(n^3)$. In addition, other SPDE discretization schemes might be considered such as Finite Elements (FEM), see e.g. [Lindgren et al., 2011], [Cameletti et al., 2013] or Finite Volumes (FVM), see e.g [Fuglstad et al., 2015c]. They are relevant when the observation dataset is not available on a regular grid and no observation operator can easily be applied to match the state space with the observation locations.

3 A surrogate SPDE-based spatio-temporal prior

In this work, we propose to use as surrogate modeling for the dynamical evolution of the spatio-temporal process $X_\theta(\mathbf{s}, t)$ a spatio-temporal SPDE prior embedding the estimation of its parametrization θ (that controls local anisotropy, correlation range, and marginal variance), see Section 5. Based on the initial results presented in Section 2, let modify the isotropic spatial SPDE to obtain a GP X as solution of a spatio-temporal SPDE:

$$\left\{ \frac{\partial}{\partial t} + (\kappa^2(\mathbf{s}, t) - \Delta)^{\alpha/2} \right\} X(\mathbf{s}, t) = \tau(\mathbf{s}, t)Z(\mathbf{s}, t) \quad (12)$$

Regarding the right-hand side noise of Eq. (12), it is assumed separable, i.e. $Z(\mathbf{s}, t) = Z_t(t) \otimes Z_s(\mathbf{s})$ with $Z_t(t)$ a temporal white noise. $Z_s(\mathbf{s})$ can also be a spatial white noise or we may consider a colored noise to ensure more regularity on process X accross time. In this case, it is taken as a solution of an isotropic spatial SPDE with precision matrix \mathbf{Q}_s :

$$(\kappa_s^2 - \Delta)^{\alpha_s/2} Z_s(\mathbf{s}) = W(\mathbf{s}) \quad (13)$$

with $W(\mathbf{s})$ a white noise with unit variance.

3.1 Spatio-temporal simulation

Let start by using a numerical implicit Euler scheme to discretize the space-time SPDE (12):

$$\frac{\mathbf{x}_{t+dt} - \mathbf{x}_t}{dt} + \mathbf{B}_{t+dt}\mathbf{x}_{t+dt} = \frac{\tau}{\sqrt{dt}}\mathbf{z}_{t+dt}$$

where \mathbf{x}_t and \mathbf{B}_t respectively denote the state space and the discrete differential operator $(\kappa^2 - \Delta)^{\alpha/2}$ at time t .

The evolution equation according to the Euler scheme is:

$$\mathbf{x}_{t+dt} = \mathbf{M}_{t+dt}\mathbf{x}_t + \mathbf{T}_{t+dt}\mathbf{z}_{t+dt} \quad (14)$$

where the noise \mathbf{z}_{t+dt} is white in space and $\mathbf{M}_{t+dt} = (\mathbf{I} + dt\mathbf{B}_{t+dt})^{-1}$ denotes the matrix operator that emulates the dynamical evolution of state \mathbf{x} from time t to $t + dt$. In this case, $\mathbf{T}_{t+dt} = \tau\sqrt{dt}\mathbf{M}_{t+dt}$ corresponds to the evolution linear model regularized by the product of the noise variance with the square root of the SPDE time step.

In case of a more general right-hand term, i.e. $\{\mathbf{z}_t, t > 0\}$ are independent realizations of colored noised driven by the spatial SPDE (13) and non-uniform regularization variance $\{\tau_t, t > 0\}$, the discretization leads to:

$$\mathbf{x}_{t+dt} = \mathbf{M}_{t+dt}\mathbf{x}_t + \tilde{\mathbf{T}}_{t+dt}\mathbf{z}_{t+dt} \quad (15)$$

where $\tilde{\mathbf{T}}_{t+dt} = \sqrt{dt}\mathbf{M}_{t+dt}\tau_t\mathbf{L}_s$ and \mathbf{L}_s stands for the Cholesky decomposition of the discretized spatial precision matrix \mathbf{Q}_s introduced by Eq. 13.

3.2 Spatio-temporal Optimal Interpolation

In the spatio-temporal OI formulation, we define an SPDE-based prior $\mathbf{x} = \{\mathbf{x}_0, \dots, \mathbf{x}_{Ldt}\}$. Complementary details on the covariance matrices of this sequential state is provided in Appendix D. From now on, $\mathbf{x}_0 \sim \mathcal{N}(\mathbf{0}, \mathbf{P}_0)$ denotes the initial state and $\mathbf{Q}_0 = \mathbf{P}_0^{-1}$ is always taken as the precision matrix obtained after a given stabilization run, i.e. the evolution of the dynamical system over N timesteps using as stationary parameters the initial parametrization θ_0 of the SPDE at time $t = 0$. We can rewrite :

$$\{\mathbf{x}_0, \dots, \mathbf{x}_{Ldt}\} = \mathbf{M}_G \begin{bmatrix} \mathbf{x}_0 \\ \mathbf{z} \end{bmatrix}$$

with $\mathbf{z} = [\mathbf{z}_1, \dots, \mathbf{z}_t]^\top$ and

$$\mathbf{M}_G = \begin{bmatrix} \mathbf{I} & 0 & 0 & 0 & 0 & \dots & 0 \\ \mathbf{M}_1 & \mathbf{T}_1 & 0 & 0 & 0 & \dots & 0 \\ \mathbf{M}_2\mathbf{M}_1 & \mathbf{M}_2\mathbf{T}_1 & \mathbf{T}_2 & 0 & 0 & \dots & 0 \\ \mathbf{M}_3\mathbf{M}_2\mathbf{M}_1 & \mathbf{M}_3\mathbf{M}_2\mathbf{T}_1 & \mathbf{M}_3\mathbf{T}_2 & \mathbf{T}_3 & 0 & \dots & 0 \\ \vdots & \ddots & \ddots & \ddots & \ddots & \ddots & 0 \\ \vdots & \ddots & \ddots & \ddots & \ddots & \ddots & 0 \\ \vdots & \ddots & \ddots & \ddots & \ddots & \ddots & \mathbf{T}_L \end{bmatrix}$$

Despite its apparent complexity, \mathbf{M}_G has a particular structure which allows to easily compute its inverse:

$$\mathbf{M}_G^{-1} = \begin{bmatrix} \mathbf{I} & 0 & 0 & 0 & 0 & \dots & 0 \\ -\mathbf{T}_1^{-1}\mathbf{M}_1 & \mathbf{T}_1^{-1} & 0 & 0 & 0 & \dots & 0 \\ 0 & -\mathbf{T}_2^{-1}\mathbf{M}_2 & \mathbf{T}_2^{-1} & 0 & 0 & \dots & 0 \\ 0 & 0 & -\mathbf{T}_3^{-1}\mathbf{M}_3 & \mathbf{T}_3^{-1} & 0 & \dots & 0 \\ 0 & \ddots & \ddots & \ddots & \ddots & \ddots & 0 \\ \vdots & \ddots & \ddots & \ddots & \ddots & \ddots & 0 \\ 0 & \ddots & \ddots & \ddots & \ddots & -\mathbf{T}_L^{-1}\mathbf{M}_L & \mathbf{T}_L^{-1} \end{bmatrix}$$

All this information is embedded in \mathbf{Q}_{xx} (Eq. 17), which is the inverse of the prior global covariance matrix \mathbf{P}_{xx} :

$$\mathbf{Q}_{xx} = \mathbf{P}_{xx}^{-1} = \begin{bmatrix} \mathbf{P}_0 & \mathbf{P}_{0,1} & \dots & \dots & \mathbf{P}_{0,L} \\ \mathbf{P}_{1,0} & \mathbf{P}_1 & \dots & \dots & \mathbf{P}_{1,L} \\ \vdots & \mathbf{P}_{2,1} & \mathbf{P}_2 & \dots & \mathbf{P}_{2,L} \\ \vdots & \ddots & \ddots & \ddots & \vdots \\ \mathbf{P}_{L-1,0} & \dots & \dots & \mathbf{P}_{L-1} & \mathbf{P}_{L-1,L} \\ \mathbf{P}_{L,0} & \mathbf{P}_{L,1} & \dots & \mathbf{P}_{L,L-1} & \mathbf{P}_L \end{bmatrix}^{-1} = \mathbf{M}_G^{-1\top} \begin{bmatrix} \mathbf{P}_0^{-1} & 0 & \dots & 0 \\ 0 & \mathbf{I} & \dots & 0 \\ \vdots & \ddots & \ddots & \vdots \\ 0 & 0 & \dots & \mathbf{I} \end{bmatrix} \mathbf{M}_G^{-1} \quad (16)$$

By denoting $\mathbf{S}_k = \mathbf{T}_k \mathbf{T}_k^\top$, we have

$$\mathbf{Q}_{xx} = \begin{bmatrix} \mathbf{P}_0^{-1} + \mathbf{M}_1^\top \mathbf{S}_1^{-1} \mathbf{M}_1 & -\mathbf{M}_1^\top \mathbf{S}_1^{-1} & 0 & 0 & 0 & \dots & 0 \\ -\mathbf{S}_1^{-1} \mathbf{M}_1 & \mathbf{S}_1^{-1} + \mathbf{M}_2^\top \mathbf{S}_2^{-1} \mathbf{M}_2 & -\mathbf{M}_2^\top \mathbf{S}_2^{-1} & 0 & 0 & \dots & 0 \\ 0 & -\mathbf{S}_2^{-1} \mathbf{M}_2 & \mathbf{S}_2^{-1} + \mathbf{M}_3^\top \mathbf{S}_3^{-1} \mathbf{M}_3 & -\mathbf{M}_3^\top \mathbf{S}_3^{-1} & 0 & \dots & 0 \\ \vdots & \ddots & \ddots & \ddots & \ddots & \ddots & \vdots \\ 0 & \ddots & \ddots & \ddots & \ddots & \ddots & 0 \\ \vdots & \ddots & \ddots & \ddots & \ddots & \ddots & 0 \\ 0 & \ddots & \ddots & \ddots & -\mathbf{S}_{L-1}^{-1} \mathbf{M}_{L-1} & \mathbf{S}_{L-1}^{-1} + \mathbf{M}_L^\top \mathbf{S}_L^{-1} \mathbf{M}_L & -\mathbf{M}_L^\top \mathbf{S}_L^{-1} \\ 0 & \ddots & \ddots & \ddots & 0 & -\mathbf{S}_L^{-1} \mathbf{M}_L & \mathbf{S}_L^{-1} \end{bmatrix} \quad (17)$$

Because of the formulation of \mathbf{M}_i and \mathbf{T}_i , the precision matrix \mathbf{Q}_{xx} with the FDM scheme also writes:

$$\mathbf{Q}_{xx} = \frac{1}{dt} \begin{bmatrix} \mathbf{P}_0^{-1} + \tilde{\mathbf{Q}}_{s,1} & -\tilde{\mathbf{Q}}_{s,1} \mathbf{M}_1^{-1} & 0 & 0 & 0 & \dots & 0 \\ -(\mathbf{M}_1^\top)^{-1} \tilde{\mathbf{Q}}_{s,1} & \mathbf{M}_1^\top \tilde{\mathbf{Q}}_{s,1} \mathbf{M}_1 + \tilde{\mathbf{Q}}_{s,2} & -\tilde{\mathbf{Q}}_{s,2} \mathbf{M}_2^{-1} & 0 & 0 & \dots & 0 \\ 0 & -(\mathbf{M}_2^\top)^{-1} \tilde{\mathbf{Q}}_{s,2} & \mathbf{M}_2^\top \tilde{\mathbf{Q}}_{s,2} \mathbf{M}_2 + \tilde{\mathbf{Q}}_{s,3} & -\tilde{\mathbf{Q}}_{s,3} \mathbf{M}_3^{-1} & 0 & \dots & 0 \\ \vdots & \ddots & \ddots & \ddots & \ddots & \ddots & \vdots \\ 0 & \ddots & \ddots & \ddots & \ddots & \ddots & 0 \\ \vdots & \ddots & \ddots & \ddots & \ddots & \ddots & 0 \\ 0 & \ddots & \ddots & \ddots & -(\mathbf{M}_{L-1}^\top)^{-1} \tilde{\mathbf{Q}}_{s,L-1} & \mathbf{M}_{L-1}^\top \tilde{\mathbf{Q}}_{s,L-1} \mathbf{M}_{L-1} + \tilde{\mathbf{Q}}_{s,L} & -\tilde{\mathbf{Q}}_{s,L} \mathbf{M}_L^{-1} \\ 0 & \ddots & \ddots & \ddots & 0 & -(\mathbf{M}_L^\top)^{-1} \tilde{\mathbf{Q}}_{s,L} & \mathbf{M}_L^\top \tilde{\mathbf{Q}}_{s,L} \mathbf{M}_L \end{bmatrix} \quad (18)$$

where $\tilde{\mathbf{Q}}_{s,t}$ is the precision matrix of the colored noise weighted by the non-uniform regularization variance τ_t .

3.3 From GP to DA formalism

All together from Sections 3.1 and 3.2 representing Gaussian Processes as a Stochastic Partial Differential Equation, we can also consider the case of noisy observations and ease the link with data assimilation formalism, see Särkkä and Hartikainen [2012], Särkkä et al. [2013], Grigorievskiy et al. [2016]. The state space model corresponding to the GP regression problem writes:

$$\begin{cases} \mathbf{x}_{t+dt} &= \mathbf{M}_{t+dt} \mathbf{x}_t + \tilde{\mathbf{T}}_{t+dt} \mathbf{z}_{t+dt} \\ \mathbf{y}_k &= \mathbf{H}_k \mathbf{x}_k + \boldsymbol{\varepsilon}_k \end{cases}$$

where \mathbf{z}_t is the m -dimensional noise process with precision matrix \mathbf{Q}_s and the evolution equation is defined by the feedback linear operator matrix \mathbf{M}_{t+dt} and the noise effect matrix $\tilde{\mathbf{T}}_{t+dt}$. \mathbf{H}_k is the observation operator at time t_k mapping the state space to the observation space and $\boldsymbol{\varepsilon}_k$ the observational error with covariance matrix \mathbf{R}_k . Based on this time-dependent notations, we also consider global observation operator \mathbf{H} with dimensions $(L \times p) \times (L \times m)$ and global observational error covariance matrix \mathbf{R} with dimensions

$(L \times p) \times (L \times p)$ as block diagonal matrices whose each block respectively contains the time-dependent observation operator and observational error covariance matrix \mathbf{H}_k and \mathbf{R}_k .

Let consider the state vector $[\mathbf{y}, \mathbf{x}]$ with covariance matrix $\tilde{\mathbf{P}}$:

$$\tilde{\mathbf{P}} = \begin{bmatrix} \mathbf{P}_{xx} & \mathbf{P}_{xx}\mathbf{H}^\top \\ \mathbf{H}\mathbf{P}_{xx} & \mathbf{H}\mathbf{P}_{xx}\mathbf{H}^\top + \mathbf{R} \end{bmatrix} \quad (19)$$

Then, the precision matrix $\tilde{\mathbf{Q}}$ of is still sparse and writes:

$$\tilde{\mathbf{Q}} = \begin{bmatrix} \mathbf{Q}_{xx} + \mathbf{H}^\top\mathbf{R}^{-1}\mathbf{H} & -\mathbf{H}^\top\mathbf{R}^{-1} \\ -\mathbf{R}^{-1}\mathbf{H} & \mathbf{R}^{-1} \end{bmatrix} \quad (20)$$

This type of formulation is close to what is done in data assimilation, except that we rewrite all the covariance-based equations in terms of precision matrix.

Rewriting Eq. (11) with observations error leads to:

$$\mathbf{x}^* = \left(\mathbf{Q}_{xx} + \mathbf{H}^\top\mathbf{R}^{-1}\mathbf{H} \right)^{-1} \mathbf{H}^\top\mathbf{R}^{-1}\mathbf{y} \quad (21)$$

whose posterior precision matrix of state \mathbf{x}^* is $\mathbf{Q}(\mathbf{x}|\mathbf{y}) = \mathbf{Q}_{xx} + \mathbf{H}^\top\mathbf{R}^{-1}\mathbf{H}$

4 Non-stationary models

When dealing with geophysical fields, using the isotropic SPDE defined in Eq. (12) as a surrogate dynamical model is not realistic. The Laplacian Δ involved in the differential operator is invariant to both translations and rotations. As a consequence, simulations based on this SPDE lead to isotropic spatio-temporal fields. A more generic class of non-stationary models generated by stochastic PDEs shall introduce some diffusion and/or advection terms. They are respectively obtained by introducing a local advection operator $\mathbf{m}(\mathbf{s}, t) \cdot \nabla$ where \mathbf{m} is a velocity field and local diffusion operator $\nabla \cdot \mathbf{H}(\mathbf{s}, t)\nabla$ where \mathbf{H} is the diffusion tensor:

$$\frac{\partial X}{\partial t} + \left\{ \kappa^2(\mathbf{s}, t) + \mathbf{m}(\mathbf{s}, t) \cdot \nabla - \nabla \cdot \mathbf{H}(\mathbf{s}, t)\nabla \right\}^{\alpha/2} X(\mathbf{s}, t) = \tau(\mathbf{s}, t)Z(\mathbf{s}, t) \quad (22)$$

This way of handling spatio-temporal non-stationarities in SPDE models has been first mentioned in the original paper of Lindgren et al. [2011], but because of the challenge of estimating the full set of space-time parameters, no works have been published to our knowledge pushing this framework into its completeness. Though, some parametrization of purely spatial diffusion process [Fuglstad et al., 2015c] or stationary advection-dominated SPDE [Clarotto et al., 2022] has been successfully applied.

Let stress that the advection-diffusion scheme is a good candidate for many geophysical datasets: this is the case in quasi-geostrophic approximation of Sea Surface Temperature (SST), see e.g. [Ubelmann et al., 2014] and Appendix D, but also in the dispersion of atmospheric pollutants [Menut et al., 2021] for instance. Then, this framework provides a generic and convenient way to bring more explainability in terms of space-time covariances of dynamical processes.

Such a model implies to estimate new parameters $\kappa(\mathbf{s}, t)$, $\mathbf{H}_{2 \times 2}(\mathbf{s}, t)$ and $\mathbf{m}_{2 \times 1}(\mathbf{s}, t) = [\mathbf{m}^1 \quad \mathbf{m}^2]^\top$, all varying across space and time along the data assimilation window. In addition, κ needs to be continuous while \mathbf{m} and \mathbf{H} additionally requires to be continuously differentiable. Regarding the diffusion tensor, we draw from the spatial statistics literature, see e.g. [Fuglstad et al., 2015a], to introduce the scalars $\gamma(\mathbf{s}, t)$, $\beta(\mathbf{s}, t)$, $\mathbf{v}_1(\mathbf{s}, t)$ and $\mathbf{v}_2(\mathbf{s}, t)$ as a generic decomposition of $\mathbf{H}(\mathbf{s}, t)$ through the equation:

$$\mathbf{H}(\mathbf{s}, t) = \begin{bmatrix} \mathbf{H}^{1,1} & \mathbf{H}^{1,2} \\ \mathbf{H}^{1,2} & \mathbf{H}^{2,2} \end{bmatrix}(\mathbf{s}, t) = \gamma(\mathbf{s}, t)\mathbf{I}_2 + \beta(\mathbf{s}, t)\mathbf{v}\mathbf{v}^\top$$

with $\mathbf{v}^\top = [\mathbf{v}_1(\mathbf{s}) \quad \mathbf{v}_2(\mathbf{s})]$, which models the diffusion tensor as the sum of an isotropic and anisotropic effects, the latter being described by its amplitude and magnitude. This is a valid decomposition for any symmetric positive-definite 2×2 matrix. This leads to the SPDE hyperparametrization θ of size $m \times L \times 8$

parameters ($\mathbf{H}^{1,2} = \mathbf{H}^{2,1}$): it grows linearly with the potentially high dimensional state space.

Using the discretization scheme already given in Eq.(14), the fractional differential operator may be discretized and replaced over time by a matrix $\mathbf{B}_t = \mathbf{A}_t^{\alpha/2}$, $t = 0, \dots, L$. This equation leads to the same linear system but the matrix \mathbf{B}_t is now the discrete operator approximating the advection-diffusion differential operator $\mathbf{A}_t = (\mathbf{A}_{k,l})_t$ in SPDE (22) raised to the power $\alpha/2$. In the case of advection-dominated SPDEs, we involve state-of-the-art upwind schemes for stabilization of the numerical system, by letting the advective transport term, which is the dominating term, collect its information in the flow direction, i.e., upstream or upwind of the point in question. All the calculation details are given in Appendix B.

In a compact formulation, using centered finite differences on the diffusion term, and by denoting $\mathbf{a}_{i,j}^{1,t,+} = \max(\mathbf{m}_{i,j}^{1,t}, 0)$, $\mathbf{a}_{i,j}^{1,t,-} = \min(\mathbf{m}_{i,j}^{1,t}, 0)$, $\mathbf{a}_{i,j}^{2,t,+} = \max(\mathbf{m}_{i,j}^{2,t}, 0)$, $\mathbf{a}_{i,j}^{2,t,-} = \min(\mathbf{m}_{i,j}^{2,t}, 0)$, the resulting UFD scheme is:

$$\begin{aligned} \mathbf{x}_{i,j}^{t+1} = & \mathbf{x}_{i,j}^t + dt \left[\kappa_{i,j}^t \mathbf{x}_{i,j}^t + \left(\mathbf{a}_{i,j}^{1,t,+} \mathbf{m}_{i,j}^{1,t,-} + \mathbf{a}_{i,j}^{1,t,-} \mathbf{m}_{i,j}^{1,t,+} \right) + \left(\mathbf{a}_{i,j}^{2,t,+} \mathbf{m}_{i,j}^{2,t,-} + \mathbf{a}_{i,j}^{2,t,-} \mathbf{m}_{i,j}^{2,t,+} \right) \right. \\ & + \mathbf{H}_{i,j}^{1,1,t} \frac{\mathbf{x}_{i+1,j}^t - 2\mathbf{x}_{i,j}^t + \mathbf{x}_{i-1,j}^t}{dx^2} + \mathbf{H}_{i,j}^{2,2,t} \frac{\mathbf{x}_{i,j+1}^t - 2\mathbf{x}_{i,j}^t + \mathbf{x}_{i,j-1}^t}{dy^2} \\ & \left. + \mathbf{H}_{i,j}^{1,2,t} \frac{\mathbf{x}_{i+1,j+1}^t - \mathbf{x}_{i+1,j-1}^t - \mathbf{x}_{i-1,j+1}^t + \mathbf{x}_{i-1,j-1}^t}{2dxdy} + \tau_{i,j}^t \mathbf{z}_{i,j}^{t+1} \right] \end{aligned}$$

4.1 Examples

Here, we provide some specific examples to show how the modifications in the fractional differential operator leads to more complex spatio-temporal anisotropies. In this four SPDE parametrizations, $\kappa = 0.33$, $\tau = 1$ and $\alpha = 4$.

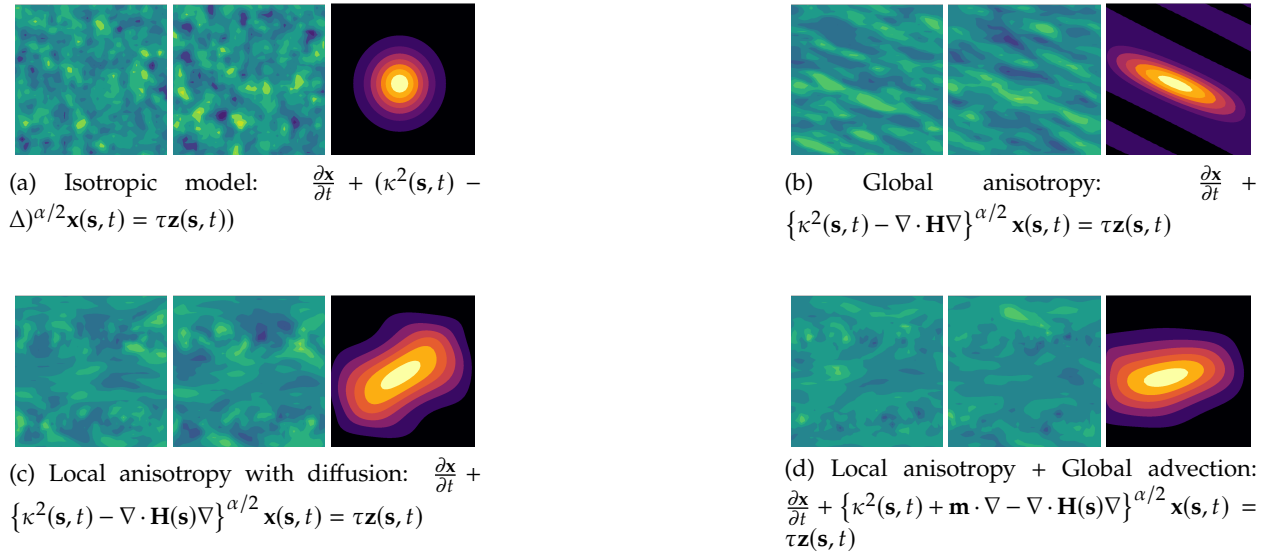


Figure 1: One realization at $t = 10$, $t = 20$ and covariance with central point of domain \mathcal{D}

5 Inference

The joint problem of estimating the best reconstruction and inferring realistic SPDE parametrizations is difficult because according to the size and nature of the dataset, the spatio-temporal interpolation may not always benefit from knowing the exact set of true SPDE parameters. Indeed, if the degree of sparsity of

the observation dataset is low, the reconstruction may be good despite a poor estimation of the covariance matrix. In the other way, if the degree of sparsity is high, much more difficult will be the estimation of the SPDE underlying parameters. In this section, we benefit from the supervised configuration of neural variational scheme to train this joint problem. In this Section, we show how to embed the global precision matrix defined by Eq. 18 in our neural scheme and define which training loss is the more appropriate to handle the bi-level optimization scheme (of both the inner variational cost and the training loss). This will lead to a stochastic version of the neural variational scheme: we estimate an SPDE-based GP prior in which we can sample ensemble members, then conditioned by the solver component of the neural architecture given the observations.

5.1 Implicit neural solvers for Optimal Interpolation

Because data assimilation is fundamentally bayesian, most of the methods used to interpolate an observational dataset involve the use of a model prior \mathbf{x} and the computation of the posterior $E[\mathbf{x}|\mathbf{y}]$ given the observations. For the latter, the computational time might be expensive, even prohibitive, because it implies to solve linear systems with matrices of high dimensions, see e.g. the precision matrix in Eqs. 17.

Recently, alternate solutions have been proposed to compute the posterior. Rather than using linear algebra, we can use a traditional variational data assimilation scheme Asch et al. [2016] and the state analysis $\mathbf{x}^* = E[\mathbf{x}|\mathbf{y}]$ is obtained by solving the minimization problem:

$$\mathbf{x}^* = \arg \min_{\mathbf{x}} \mathcal{J}(\mathbf{x})$$

where the variational cost function $\mathcal{J}(\mathbf{x}) = \mathcal{J}_{\Phi}(\mathbf{x}, \mathbf{y}, \Omega)$ is generally the sum of an observation term and a regularization term involving an operator Φ which is typically a dynamical prior:

$$\begin{aligned} \mathcal{J}_{\Phi}(\mathbf{x}, \mathbf{y}, \Omega) &= \mathcal{J}^o(\mathbf{x}, \mathbf{y}, \Omega) + \mathcal{J}_{\Phi}^b(\mathbf{x}) \\ &= \|\mathcal{H}(\mathbf{x}) - \mathbf{y}\|_{\Omega}^2 + \lambda \|\mathbf{x} - \Phi(\mathbf{x})\|^2 \end{aligned} \quad (23)$$

with \mathcal{H} the observation operator and λ_1 is a predefined or learnable scalar weight. This formulation of functional $\mathcal{J}_{\Phi}(\mathbf{x}, \mathbf{y}, \Omega)$ directly relates to strong constraint 4D-Var Carrassi et al. [2018].

When both prior $\Phi(\mathbf{x}) = \mathbf{x}^f$ and observations \mathbf{y} are assumed to be Gaussian with covariance matrices \mathbf{P} and \mathbf{R} , $\mathcal{J}_{\Phi}(\mathbf{x}, \mathbf{y}, \Omega)$ can be written:

$$\mathcal{J}_{\Phi}(\mathbf{x}, \mathbf{y}, \Omega) = (\mathbf{H}\mathbf{x} - \mathbf{y})^{\top} \mathbf{R}^{-1} (\mathbf{H}\mathbf{x} - \mathbf{y}) + \lambda (\mathbf{x} - \mathbf{x}^f)^{\top} \mathbf{P}^{-1} (\mathbf{x} - \mathbf{x}^f) \quad (24)$$

This is well known that equating to zero the gradient of this cost function at a single time t_k produces the exact same analysis formulation that the Kalman Filter analysis step or the BLUE/simple kriging equations.

For inverse problems with time-related processes, the minimization of functional \mathcal{J}_{Φ} usually involves iterative gradient-based algorithms and in particular request to consider the adjoint method in classic equation-based variational data assimilation schemes [Asch et al., 2016] where operator Φ identifies to a deterministic model $\mathbf{x}_{k+1} = \mathcal{M}(\mathbf{x}_k)$:

$$\mathbf{x}^{(i+1)} = \mathbf{x}^{(i)} - \alpha \nabla_{\mathbf{x}} \mathcal{J}_{\Phi}(\mathbf{x}^{(i)}, \mathbf{y}, \Omega)$$

[Fablet et al., 2020] shows that an end-to-end deep learning framework can be built based on the above variational formulation where both prior operator Φ and solver Γ , i.e. the operator solving for the gradient-based minimization of the variational cost, are neural networks. For the latter, following meta-learning schemes [Andrychowicz et al., 2016], a residual LSTM-based representation of operator Γ is considered where the i^{th} iterative update of the solver is given by:

$$\begin{cases} \mathbf{g}^{(i+1)} &= LSTM [\alpha \cdot \nabla_{\mathbf{x}} \mathcal{J}_{\Phi}(\mathbf{x}^{(i)}, \mathbf{y}, \Omega), h(i), c(i)] \\ \mathbf{x}^{(i+1)} &= \mathbf{x}^{(i)} - \mathcal{T}(\mathbf{g}^{(i+1)}) \end{cases} \quad (25)$$

with $\mathbf{g}^{(i+1)}$ is the LSTM output using as input gradient $\nabla_{\mathbf{x}} \mathcal{J}_{\Phi}(\mathbf{x}^{(i)}, \mathbf{y}, \Omega)$, while $h(i)$ and $c(i)$ denotes the internal states of the LSTM [Arras et al., 2019], α is a normalization scalar and \mathcal{T} a linear or convolutional

mapping.

In this formulation, the prior term Φ is jointly estimated so that the reconstruction fulfills at most the outer loss function \mathcal{L} used during the training process. Typically, such a loss function may be stated as:

$$\mathcal{L}(\mathbf{x}, \mathbf{x}^*) = \|\mathbf{x} - \mathbf{x}^*\|^2 + \mathcal{L}_{regul}, \quad (26)$$

the mean squared error between the reconstruction and the ground truth, with additional regularization terms. This implies a bi-level optimization scheme of both the inner variational cost and the outer training loss function.

Though, the prior Φ is not easily interpretable: it just acts as an encoding of the state \mathbf{x} that helps in the gradient-based minimization process. In this work, we aim at bringing both explainability and stochasticity in the neural scheme by considering as a surrogate model for Φ an SPDE instead of a given neural-based architecture. To do so, let start by making an explicit link between the variational formulation of OI and 4DVar, see e.g. Beauchamp et al. [2023c]. Let rewrite the matrix formulation of the regularization prior term of Eq. 23 as:

$$\mathbf{x}^\top \mathbf{P}^{-1} \mathbf{x} = \mathbf{x}^\top \mathbf{S}^\top \mathbf{S} \mathbf{x} = \|\mathbf{S} \mathbf{x}\|^2 = \|\mathbf{x} - \Phi(\mathbf{x})\|^2$$

with $\Phi = (1 - \mathbf{S})$, and \mathbf{S} is the square root of the precision matrix \mathbf{Q}_G defined by Eq. 18. When operator Φ is linear, which is the case when discretizing the fractional operator of a linear SPDE, equating the gradient of this cost function to zero leads to the optimal solution (gaussian case):

$$\mathbf{x}^* = \left(\mathbf{1}_\Omega + \lambda \Phi^\top + \lambda \Phi^\top \Phi \right)^{-1} \mathbf{y}$$

for $\mathcal{H} = \mathbf{1}_\Omega$. In this formulation of the optimal interpolation, it is clear that if the prior precision matrix \mathbf{Q} is known, it can easily be embedded in the inner variational cost used by the LSTM iterative solver to optimize the outer training loss function. Still, the prior SPDE-based covariance is usually unknown. In the next Section, we propose an end-to-end architecture to estimate jointly the SPDE-based prior parameters together with the optimal reconstruction of the state.

5.2 Deep learning joint parameters inference and reconstruction

Finding the best set parameters of the SPDE to optimize the reconstruction and helps to uncertainty quantification may be intricate. Drawing from the usual neural variational framework, the trainable prior is now SPDE-based, and the parameters $\theta = [\kappa \quad \mathbf{m} \quad \mathbf{H} \quad \tau]^\top$ are now embedded in an augmented state formalism, i.e.:

$$\tilde{\mathbf{x}} = [\mathbf{x} \quad \theta]^\top \quad (27)$$

The latent parameter θ is potentially non stationary in both space and time and its size is directly related to the size of the data assimilation window L . Because κ , τ and γ (in the decomposition of the diffusion term, see Section 4) are both strictly positive, we use ReLu activation function on these three parameters to ensure their consistency.

For the training process, we may consider different loss functions:

- $\mathcal{L}_1(\mathbf{x}, \mathbf{x}^*) = \|\mathbf{x} - \mathbf{x}^*\|^2$ is the L2-norm of the difference between state \mathbf{x} and reconstruction \mathbf{x}^*
- $\mathcal{L}_2(\mathbf{x}, \hat{\theta}) = -\log|\mathbf{Q}(\hat{\theta})| + \mathbf{x}^\top \mathbf{Q}(\hat{\theta}) \mathbf{x}$ is the negative log-likelihood of the true states given the estimated precision matrix $\mathbf{Q}(\hat{\theta})$, thus ensuring consistency between the actual ground truth and the SPDE parameters.

Using \mathcal{L}_1 will lead to satisfactory reconstructions without any constraints on the SPDE parameters. The single use of \mathcal{L}_2 should lead to satisfactory results if the analytical solver, i.e. the inversion of the linear system or the gradient-based minimization of the variational cost, were used. But because the solver is trained, it also needs to be constrained by an appropriate loss function for the reconstruction, meaning \mathcal{L}_1 .

The best solution is then to create a mixed loss function, combination of \mathcal{L}_2 to estimate at best the SPDE parameters and optimize the prior model, and \mathcal{L}_1 to satisfy the reconstruction criteria and optimize the solver.

The log-determinant of the precision matrix $\log |\mathbf{Q}(\hat{\theta})|$ is usually difficult to handle when computing \mathcal{L}_2 . Hopefully, based on the particular structure and the notations already introduced for the spatio-temporal precision matrix \mathbf{Q} in Eq.(17), it writes, see e.g. Clarotto et al. [2022]:

$$\begin{aligned}
 \log |\mathbf{Q}(\hat{\theta})| &= \log |\mathbf{P}_0^{-1}| + \log |\mathbf{S}_1^{-1}| + \dots + \log |\mathbf{S}_L^{-1}| \\
 &= \log |\mathbf{P}_0^{-1}| + \sum_{i=1}^L \log (|\mathbf{L}_i \mathbf{L}_i^T|) \\
 &= \log |\mathbf{P}_0^{-1}| + 2 \sum_{i=1}^L \sum_{j=1}^m \log \mathbf{L}_i(j, j)
 \end{aligned} \tag{28}$$

where \mathbf{L}_i denotes here the Cholesky decomposition of \mathbf{S}_k^{-1} .

Overall, let denote by $\Psi_{\theta, \Gamma}(\tilde{\mathbf{x}}^{(0)}, \mathbf{y}, \Omega)$ the output of the end-to-end learning scheme given the SPDE-based dynamical model with parameters θ and the neural residual architecture for the solver Γ , see Figure 2 and Algorithm 1, the initialization $\tilde{\mathbf{x}}^{(0)}$ of augmented state $\tilde{\mathbf{x}}$ and the observations \mathbf{y} on domain Ω .

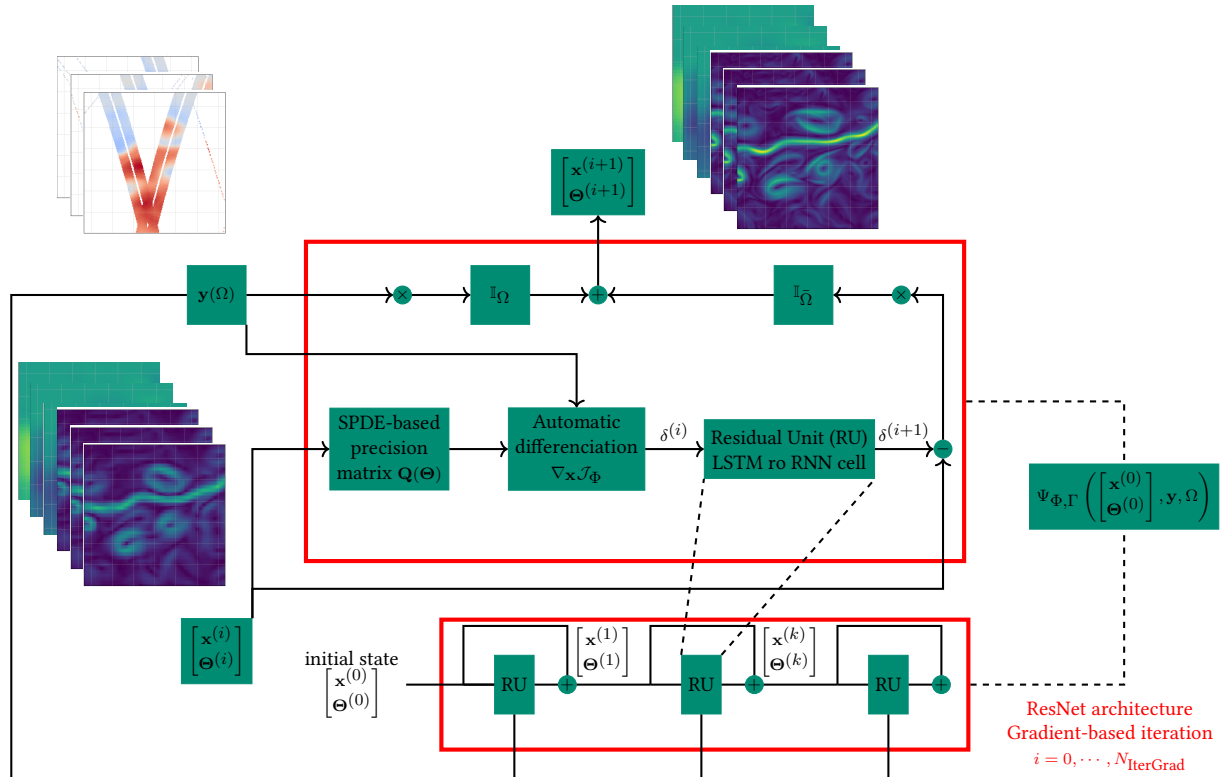


Figure 2: Sketch of the gradient-based algorithm. \mathbf{I}_{Ω} acts as a masking operator for any spatio-temporal location not in Ω .

Algorithm 1: Variational scheme with SPDE-based GP prior and implicit neural solver

Data :

$$\mathbf{x} \in \mathbb{R}^{T \times m} = \{\mathbf{x}_k\}, k = 1, \dots, T$$

$$\mathbf{y}_\Omega = \{\mathbf{y}_{k, \Omega_k}\}, k = 1, \dots, T: \text{ observations on domains } \Omega_k \subset \mathcal{D}$$

N_I : number of iterations

η : gradient step

Init :

$$\tilde{\mathbf{x}}^{*(0)}$$

List of procedures :

$\text{Train_}\Psi_{\theta, \Gamma}$: end-to-end learning procedure with:

θ : parameter of the SPDE-based prior operator;

GradLSTM : residual NN-based representation of $\nabla_{\mathbf{x}} \mathcal{J}(\mathbf{x})$

Γ : iterative gradient-based update operator:

$$i = 0$$

while $i < N_I$ **do**

$$\left| \begin{array}{l} \mathbf{Q}_G(\hat{\theta}^{(i)}) = \mathbf{P}_G^{-1}(\hat{\theta}^{(i)}) = \mathbf{M}_G^{-1}(\hat{\theta}^{(i)})^\top \begin{bmatrix} \mathbf{P}_0^{-1} & 0 & \dots & 0 \\ 0 & \mathbf{I} & \dots & 0 \\ \vdots & \ddots & \ddots & \vdots \\ 0 & 0 & \dots & \mathbf{I} \end{bmatrix} \mathbf{M}_G^{-1}(\hat{\theta}^{(i)}) \\ \tilde{\mathbf{x}}^{(i+1)} \leftarrow \tilde{\mathbf{x}}^{(i)} - \eta \times \text{GradLSTM}(\tilde{\mathbf{x}}^{(i)}) \\ N_I \nearrow; \eta \searrow; i \leftarrow i + 1 \end{array} \right.$$

end

for $i \in 0, \dots, n_{epochs}$ **do**

$$\left| \begin{array}{l} \omega_{\Psi_{\theta, \Gamma}}^{(i+1)} \leftarrow \omega_{\Psi_{\theta, \Gamma}}^{(i)} - lr \times \nabla \mathcal{L}(\mathbf{x}, \mathbf{x}^{*(i)}, \theta^{(i)}) \end{array} \right.$$

end

Result : $\tilde{\mathbf{x}}^* \leftarrow \Psi_{\theta, \Gamma}(\tilde{\mathbf{x}}^{(0)}, \mathbf{y}, \Omega)$

Then, the joint learning for the weights $\omega_{\theta, \Gamma}$ of the neural scheme given the SPDE formulation that is chosen (isotropic or not, non-stationary or not, etc.) and the architecture of operator Γ is stated as the minimization of the mixed loss function:

$$\hat{\omega}_{\Psi_{\theta, \Gamma}} = \arg \min_{\theta, \Gamma} \left[\lambda_1 \mathcal{L}_1(\mathbf{x}^*, \mathbf{x}) + \lambda_2 \mathcal{L}_2(\mathbf{x}, \hat{\theta}) \right] \text{ s.t. } \tilde{\mathbf{x}}^* = \Psi_{\theta, \Gamma}(\tilde{\mathbf{x}}^{(0)}, \mathbf{y}, \Omega) \quad (29)$$

In case of unsupervised learning, the same strategy may apply but \mathcal{L}_2 will be the likelihood of the observations given the estimated SPDE parameters since in this case, the true states would not be available during the training process.

5.3 Implementation aspects

Regarding the implementation of our model, we use Pytorch [Paszke et al., 2017] whose sparse linear algebra is not providing yet a sparse Cholesky algorithm and a sparse solver of linear systems, which is critical, especially when computing the likelihood \mathcal{L}_2 in the training loss function. As a consequence, despite the theoretical tools have been fully detailed in the previous sections, we had to implement new functionalities based on scipy sparse linear algebra [Virtanen et al., 2020] to store the precision matrices in an efficient way and compute the inner variational cost, see again Eq.23. In particular, we provide a PyTorch extension of sparse cholesky matrices, see Appendix B, based on the CHOLMOD supernodal Cholesky factorization [Chen et al., 2008] and draw from Seeger et al. [2019] to provide the backward pass of the sparse Cholesky decomposition.

Also, let stress that such as sparse formulation is key in the memory-saving component of the algorithm because it relies on a set of N_{iter} gradient-based iterations, meaning that for a single interpolation task, the precision matrix $\mathbf{Q}(\theta^{(i)})$ is stored N_{iter} times along the computational graph with updated values of the SPDE parameters $\theta^{(i)}$.

6 Related and future works

6.1 From generative models ...

The targeted interpolation problem, stated as the sampling of the posterior pdf of a state given some partial observations, relates to conditional generative models, where the conditioning results from the partial observations. Generative models have received a large attention in the deep learning literature with a variety of neural schemes including among others GANs [Goodfellow et al., 2014], VAEs [Kingma and Welling, 2022], normalizing flows [Dinh et al., 2017] and diffusion models [Ho et al., 2020]. We discuss further these connections below.

As we rely on SPDE-based state-space formulations, we can make explicit the gradient of the inner variational cost $\mathcal{J}(\mathbf{x}, \mathbf{y}, \Omega)$. Considering a covariance matrix \mathbf{R} for the observation noise, we can derive the following expression:

$$\begin{aligned} \nabla_{\mathbf{x}} \mathcal{J}(\mathbf{x}, \mathbf{y}, \Omega) &= \nabla_{\mathbf{x}} [\mathbf{d}^T \mathbf{R}^{-1} \mathbf{d} + \mathbf{x}^T \mathbf{Q}^{-1} \mathbf{x}] = -\mathbf{H}_{\Omega}^T \mathbf{R}^{-1} \mathbf{d} + \mathbf{Q}^{-1} \mathbf{x} \\ &= \nabla_{\mathbf{x}} \log p(\mathbf{y} | \mathbf{x}) + \nabla_{\mathbf{x}} \log p(\mathbf{x}) \end{aligned} \quad (30)$$

where $\mathbf{d} = \mathbf{y} - \mathbf{H}_{\Omega} \mathbf{x}$. Score-based approaches [Sohl-Dickstein et al., 2015] exploits similar formulations. However, they directly parameterize the gradient of the likelihoods rather than the likelihoods themselves. Here, we exploit the latter through an observation operator and the SPDE prior. Another important difference with score-based approaches lies in the considered gradient-based procedure to sample the posterior. Score-based schemes generally rely on Langevin dynamics [Grenander and Miller, 1994] *i.e.* a stochastic gradient descent for posterior $\mathbf{x} | \mathbf{y}$. Here, we exploit a gradient-based LSTM solver similarly to trainable optimizers exploited in meta-learning schemes [Andrychowicz et al., 2016]. This greatly speeds up the convergence of the inner minimization and allows us to train the overall neural scheme end-to-end. As we do not exploit a stochastic solver, our ability to sample the posterior does not derive from the implementation of Langevin dynamics but we exploit the analytic form of the SPDE to sample in the prior. Future works could explore further whether Langevin dynamics fits within the proposed framework.

In Eq.(30), we could consider using only the regularization cost if we are only interested to learn SPDE surrogate generative models using as training data gap-free states. In such a case, the proposed formulation relates to variational autoencoder (VAE) formulations [Kingma and Welling, 2022], see also Fig.3b), in which the encoder projects the state \mathbf{x} to the parameter space θ . The encoder is trained on the NLL of θ . The decoder is simply the SPDE, and does not require any training. Back to the encoder part, it may compress the original high-dimensional input space into a lower-dimensional space, if the SPDE is stationary for instance. More generally, when complex spatio-temporal anisotropies are involved, and without a parametrization model for the latent variable θ , the latter has high dimensionality (same as the original data or higher), as it is done in diffusion-based models, see e.g. [Sohl-Dickstein et al., 2015, Ho et al., 2020]. Along this line, starting from any initial conditions θ_0 , the optimal set of parameters θ^* (given \mathbf{x}) would be obtained by the iterations:

$$\theta_i = \theta_{i+1} - \mathcal{K} [\rho \nabla_{\theta} \log p(\mathbf{x} | \theta)]$$

because the target cost function would not be the 4DVar cost anymore but its regularization part (prior cost), *i.e.* $\log p(\mathbf{x} | \theta)$. As already said above, this relates to Langevin dynamics formalism.

Eq.(22) provides a simple way to generate SPDE-driven GP simulations starting from white or colored noise \mathbf{z}_0 . It can be seen as the so-called reverse process in diffusion-based models [Ho et al., 2020]. Because we deal with space-time processes, this reverse process would actually go forward in time, while the corresponding forward process would go backward in time till the initial noise used in the SPDE to generate realistic space-time sequences. Considering our formulation, the reverse process can be reformulated as follows:

$$\mathbf{x}_{i+1} = \mathbf{M}_{i+1} \mathbf{x}_i + \mathbf{T}_{i+1} \mathbf{z}_i = \mathbf{x}_i - \mathbf{F}_{i+1} \mathbf{M}_{i+1} \mathbf{x}_i + \mathbf{T}_{i+1} \mathbf{z}_i \quad (31)$$

because of the Woodbury matrix identity $\mathbf{M}_{i+1} = \mathbf{I} - \mathbf{F} \mathbf{M}_{i+1}$. By [Anderson, 1982], we also know that given a forward process (data to noise):

$$\mathbf{x}_i = \mathbf{x}_{i+1} + \mathbf{f}_{i+1}(\mathbf{x}_{i+1}) + \mathbf{G}_{i+1} \mathbf{z}_{i+1}$$

the corresponding reverse process (noise to data) writes:

$$\mathbf{x}_{i+1} = \mathbf{x}_i + \mathbf{f}_i(\mathbf{x}_i) - \frac{1}{2} \nabla \cdot [\mathbf{G}_i \mathbf{G}_i^T] - \frac{1}{2} \mathbf{G}_i \mathbf{G}_i^T \nabla \log p_i(\mathbf{x}_i) + \mathbf{G}_i \mathbf{z}_i$$

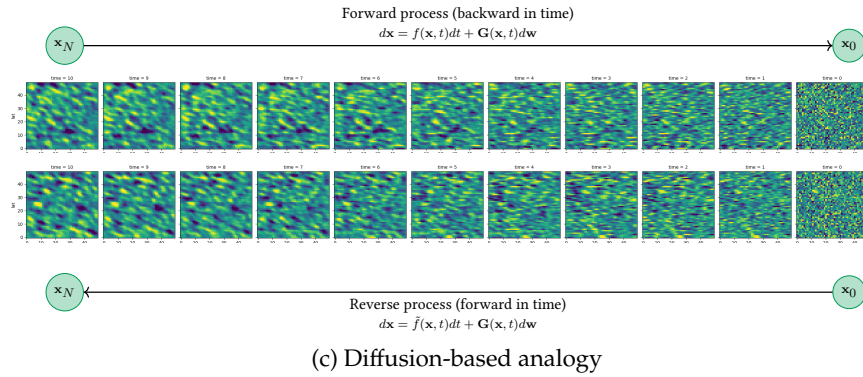
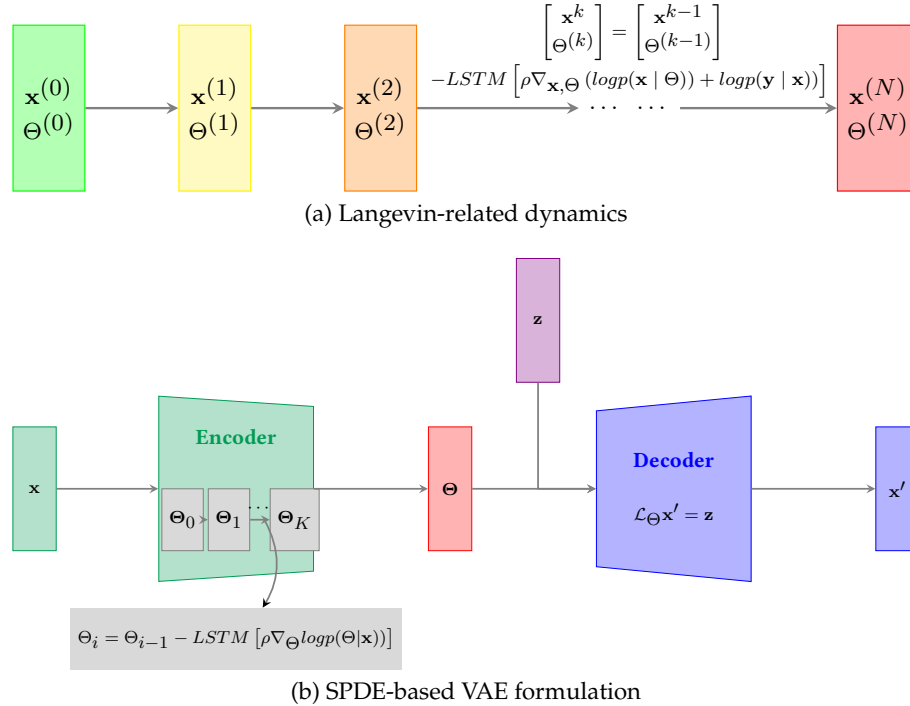


Figure 3: Example of analogies between our combination of SPDE prior and neural solver with generative models

Then, by simple identification, the drift term $\mathbf{f}_i(\mathbf{x}_i)$ is:

$$\mathbf{f}_i(\mathbf{x}_i) = -\mathbf{F}_{i+1}\mathbf{M}_{i+1} + \frac{1}{2}\nabla \cdot [\mathbf{T}_{i+1}\mathbf{T}_i^\top] + \frac{1}{2}\mathbf{T}_{i+1}\mathbf{T}_{i+1}^\top \mathbf{P}_{i+1}^{-1}\mathbf{x}_{i+1} \quad (32)$$

since $\nabla \log p_{i+1}(\mathbf{x}_{i+1}) = -\mathbf{P}_{i+1}^{-1}\mathbf{x}_{i+1}$ Fig.3c) demonstrates this link when simulating with Eq. (31) a GP with global anisotropy on a uniform Cartesian grid with dx , dy and dt all set to one and shows how we can retrieve the forward process from Eq. (32). This opens a new challenge for future work to estimate the underlying stochastic differential equation of the forward process for space-time sequences, then being able to generate realistic space-time dynamics.

6.2 To ensemble-based extensions

Because the PDE is stochastic, it provides an easy way to generate a set of N realizations \mathbf{x}_i , $i = 1, \dots, N$, conditioned by the observations available \mathbf{y} , as a way of estimating both mean and uncertainty of the state \mathbf{x} . We draw from traditional geostatistics to realize SPDE-based spatio-temporal non conditional simulations with a kriging-based conditioning [Wackernagel, 2003]. Except that we replace the kriging algorithm by our

neural approach, which has to be seen as a generic interpolation tool. Because the latter acts by construction as a smoother of the hidden truth, an option to retrieve the original variability of the underlying process is to run conditional simulations \mathbf{x}_c that writes:

$$\mathbf{x}^{*,i}(\mathbf{s}, t) = \mathbf{x}^*(\mathbf{s}, t) + (\mathbf{x}_s^i(\mathbf{s}, t) - \mathbf{x}_s^{*,i}(\mathbf{s}, t)) \quad (33)$$

where \mathbf{x}^* denotes the neural-based interpolation, \mathbf{x}_s^i is an SPDE simulation of the process \mathbf{x} based on the parameters $\hat{\theta}$ and $\mathbf{x}_s^{*,i}$ is the neural reconstruction of this non-conditional simulation, using as pseudo-observations a subsampling of \mathbf{x}_s^i based on the actual data locations. Because $E[\mathbf{x}_s^i - \mathbf{x}_s^{*,i}] = 0$, the resulting simulation is well conditioned by the observations at data locations.

Running an ensemble of N conditional simulations gives an approximation of the probability distribution function $p_{\mathbf{x}|\mathbf{y}}$ of state $\mathbf{x}|\mathbf{y} = \{\mathbf{x}_0|\mathbf{y}, \dots, \mathbf{x}_L|\mathbf{y}\}$. The ensemble mean $\overline{\mathbf{x}^{*,i}}$ will be \mathbf{x}^* in the limits of $N \rightarrow +\infty$:

$$\frac{1}{N} \sum_i \mathbf{x}^{*,i}(\mathbf{s}, t) \xrightarrow{N \rightarrow +\infty} \mathbf{x}^*(\mathbf{s}, t)$$

Such an approach has already been successfully tested in [Beauchamp et al., 2023a] when using analog operator strategy [Tandeo et al., 2015] to draw non-conditional simulation in the prior distribution.

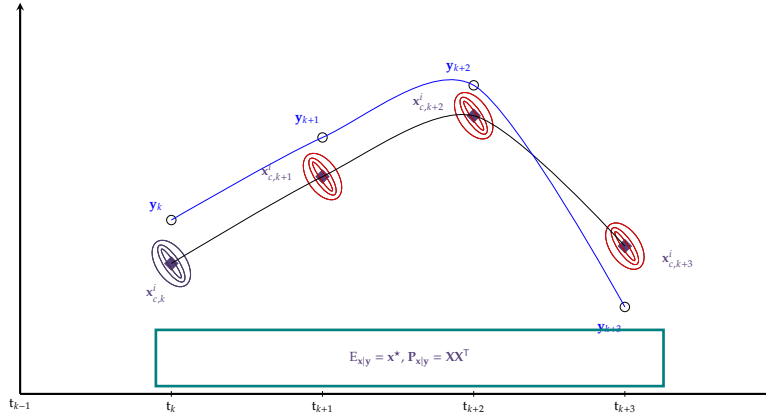


Figure 4: Ensemble-based neural variational scheme with SPDE-based GP prior: the assimilation is not sequential. The inversion scheme embeds the global precision matrix of the state sequence $\{\mathbf{x}_0, \dots, \mathbf{x}_{Ldt}\}$ in the inner variational cost to minimize. Ensemble members are generated from the Gaussian prior surrogate SPDE model, then conditioned by the neural solver so that the posterior pdf is no longer Gaussian. The posterior pdf is empirically ensemble-based computed: $P_{\mathbf{x}|\mathbf{y}} = \mathbf{X}\mathbf{X}^T$ with $\mathbf{X} = (1/\sqrt{N-1}) [\mathbf{x}^{*,i} - \mathbf{x}^*]$

Let note that in this formulation, the idea is to run SPDE-based conditional simulation of the prior Matérn field $\mathbf{x}(\mathbf{s}, t)$. One ensemble member is obtained by running one space-time simulation, and two space-time neural reconstructions along the data assimilation window, then combined through Equation 33. As a consequence, there is no sequential assimilation. Though, in the idea, such a conditioning is exactly similar to the one produced by EnKF simulations: in geostatistical terms we can interpret the forecast step of the EnKF as being unconditional simulations at time $t-1$ generating N realizations of a non-stationary random function (SPDE-based here) for time t . Both prior mean and covariance matrix are then computed directly on this set of unconditional realizations, before the analysis step, i.e. their conditioning with the observations. The key advantage of the EnKF is its flow-dependency that propagates the uncertainties at each time step with the evolution model, while the classic EnOI method generally used by geoscientists, see e.g. Asch et al. [2016], Counillon and Bertino [2009] replaces the flow-dependent EnKF error covariance matrix by a stationary matrix calculated from an historical ensemble. This is an important difference with our approach: while the neural architecture can be seen as a way to learn neural ensemble-based optimal interpolation models and solvers, our GP prior encoded by its SPDE precision matrix, built according to the FDM scheme with varying parameters over space and time, still allows for flow dependency, based on the learning of the SPDE parametrization given the input observations.

7 Application

In this Section, we provide two applications of this work:

- The first example relies on a spatio-temporal GP simulation driven by a non-stationary spatial diffusion tensor. Because the dynamical process is linear, the best reconstruction is provided by the optimal interpolation using the SPDE parameters used in the simulation to fill in the precision matrix.
- The second example uses an Observation System Simulation Experiment (OSSE) of the Sea Surface Height (SSH) along the Gulf Stream. We will use the SPDE-based prior as a surrogate model along the data assimilation window to provide ensemble members of the posterior distribution.

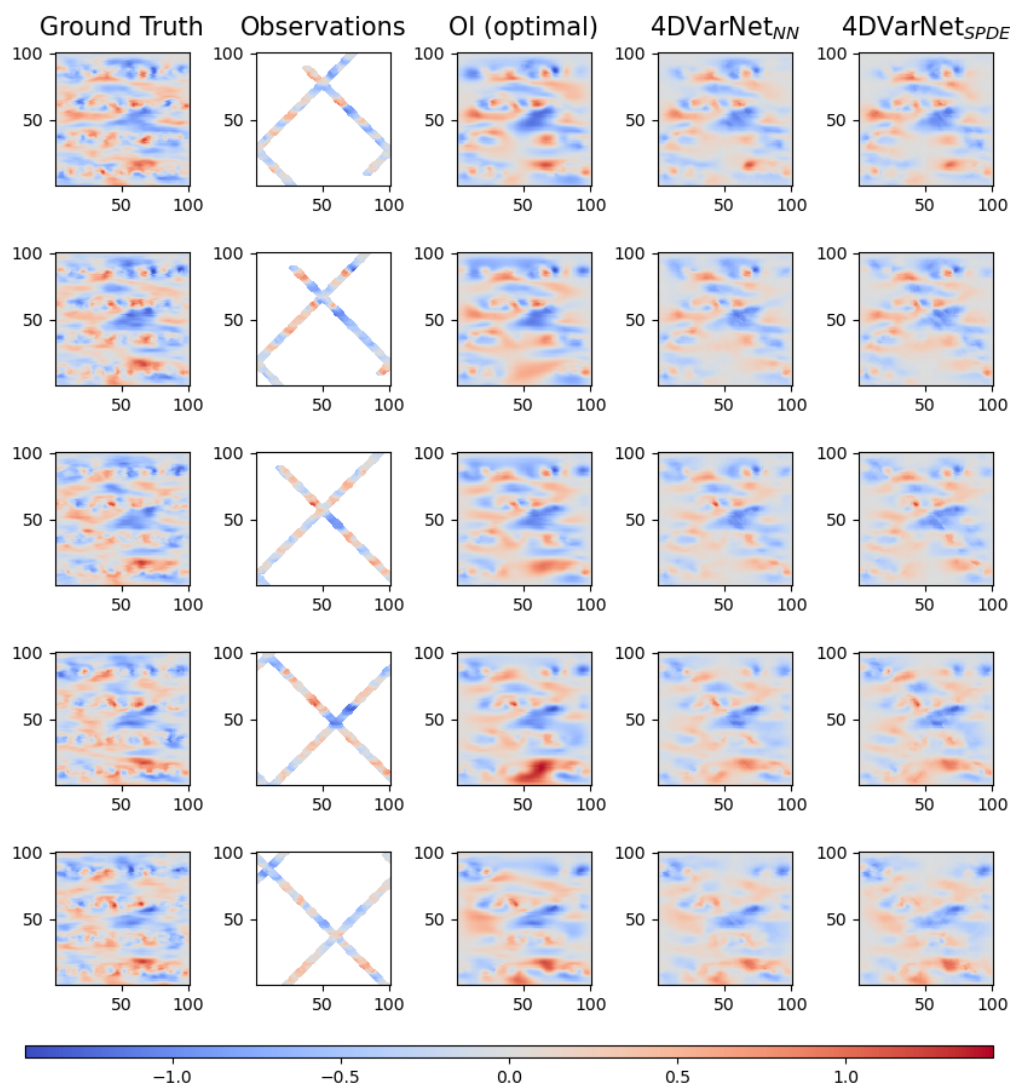


Figure 5: From left to right: Ground Truth, Pseudo-observations, Optimal Interpolation, neural variational scheme with UNet-based and SPDE-based prior operator Φ . A data assimilation window of length 5 is used

Example 7.1 Diffusion-based non stationary GP. In this first application, we simulate 500 states of a GP driven by the following diffusion SPDE:

$$\{\kappa^2 - \nabla \cdot \mathbf{H}(\mathbf{s})\nabla\}^{\alpha/2} \mathbf{x}(\mathbf{s}, t) = \tau \mathbf{z}(\mathbf{s}, t) \quad (34)$$

The regularity parameter $\kappa = 0.33$ is fixed over space and time. To ensure the GP to be smooth enough, we use a value of $\alpha = 4$. Such a formulation enables to generate GPs driven by local anisotropies in space leading to non stationary spatio-temporal fields with eddy patterns. The diffusion tensor \mathbf{H} is a 2-dimensional diffusion tensor generated by drawing from the spatial statistics literature, see e.g. [Fuglstad et al., 2015a]. We introduce a generic decomposition of $\mathbf{H}(\mathbf{s}, t)$ through the equation:

$$\mathbf{H} = \gamma \mathbf{I}_2 + \beta \mathbf{v}(\mathbf{s})^T \mathbf{v}(\mathbf{s})$$

with $\gamma = 1$, $\beta = 25$ and $\mathbf{v}(\mathbf{s}) = (v_1(\mathbf{s}), v_2(\mathbf{s}))^T$ using a periodic formulation of its two vector fields components, see Section 4. We use the Finite Difference Method in space coupled with an implicit Euler scheme in time to solve for the equation. Let $\mathcal{D} = [0, 100] \times [0, 100]$ be the square spatial domain of simulation and $\mathcal{T} = [0, 500]$ the temporal domain. Both spatial and temporal domains are discretized so that the simulation is made on a uniform Cartesian grid consisting of points (x_i, y_j, t_k) where $x_i = i\Delta x$, $y_j = j\Delta y$, $t_k = k\Delta t$ with Δx , Δy and Δt all set to one.

We train the neural architectures for both UNet-based and SPDE-based priors with Adam optimizer on 50 epochs. The training period goes from timestep 100 to 400. During the training procedure, we select the best model according to metrics computed over the validation period from timestep 30 to 80. Overall, the set of metrics is computed on a test period going from timestep 450 to 470. No further improvements in the training losses are seen when training the model longer. We use a data assimilation window of length 5 and generate pseudo-observations from the ground truth, inspired by orbiting satellites tracks around the earth, see Example 7.2. Figure 5 displays the results obtained by Optimal Interpolation and the neural implicit solver with both UNet and SPDE-based parametrization of the prior. Neural-based reconstructions are optimized at the center of the assimilation window ($T = 2$), which is why the performance may be affected for other leadtime. There is no significant differences between the two prior formulations used in the neural scheme, which overall retrieve the main patterns of the OI. Some artefacts may appear due to the observation term in the inner variational cost that tends to lead the solution towards the observation in its close neighbourhood. Improvements may be expected when adding regularization terms in the training loss to counteract such effects, see e.g. [Beauchamp et al., 2023b]. Regarding the derived framework proposed in this work, one of the question was: is it possible to retrieve interpretable SPDE parametrizations from the joint learning setting? Two configurations were considered: when using as initial condition for the parametrization a gradient-based information of the accumulated alongtrack observations, i.e. $\mathbf{H}_{11} = \nabla_{\vec{x}} \mathbf{y}$ and $\mathbf{H}_{22} = \nabla_{\vec{y}} \mathbf{y}$; or an isotropic initialization, i.e. $\mathbf{H} = \mathbf{I}$. The first configuration enables to identify patterns in zonal and meridional components of the true diffusion tensor and leads to an optimal parametrization θ^* very close to the true diffusion tensor. While leading to different SPDE parametrizations θ^* , the interpolation metrics are similar in the end for the two initializations. In addition, using an isotropic initial condition is more general (see the next realistic SSH application) and also retrieves in the end the main zonal flow directions encoded by \mathbf{H}_{22} , while the meridional and periodic structures of \mathbf{H}_{11} and \mathbf{H}_{12} are partly seen as well.

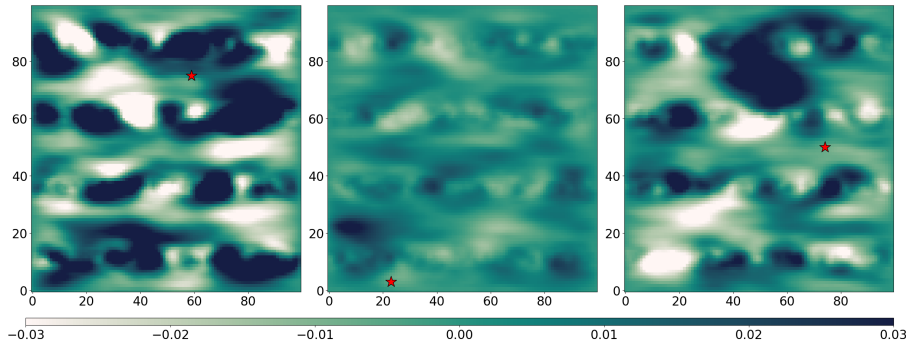


Figure 6: Estimated prior covariance between the three locations \mathbf{s} (red stars) at the center of assimilation window (time=2) and the other points of domain \mathcal{D}

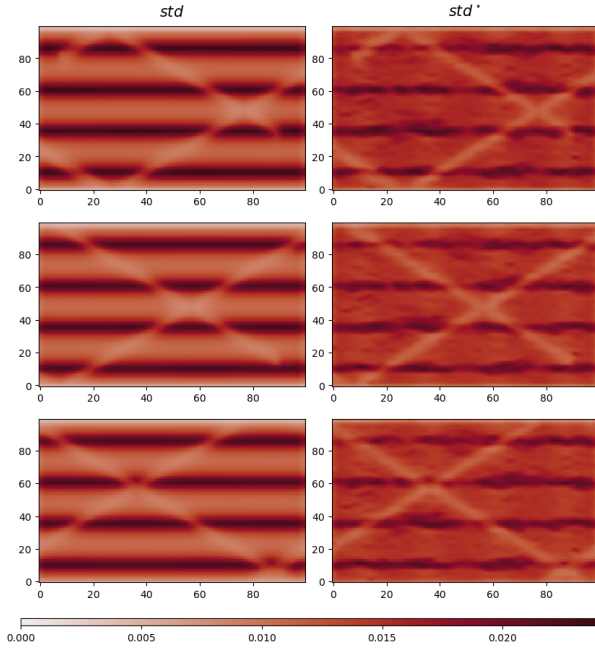


Figure 7: True (left) and estimated (right) posterior standard deviations at the beginning, center and end of the assimilation window $time = 0, 2, 4$

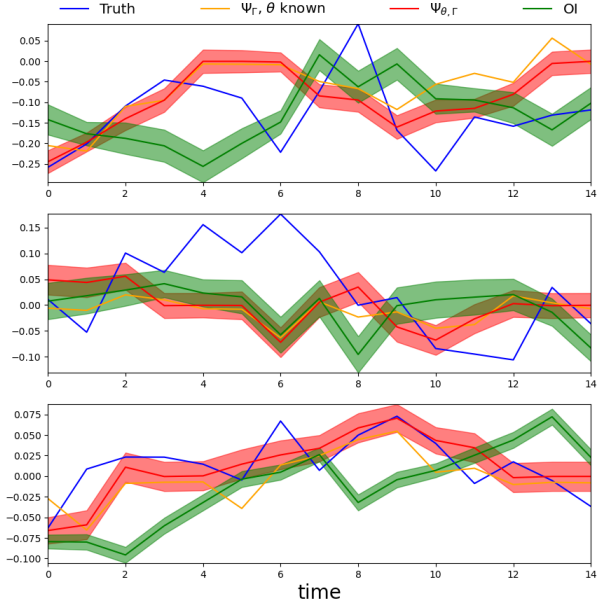


Figure 8: Ground truth, OI and its posterior variance (blue), neural scheme with SPDE parametrization θ known (orange) and with inference of θ (red) for the same three points identified in Figure 6 along the 15 days test period

Looking at the estimated spatio-temporal prior covariance matrices based on the isotropic initial condition for three different points (red stars) $\in \mathcal{D}$, see Figure 6, we understand that even if the initial set of parameters is not retrieved, they still remain interpretable in terms of how the GP prior covariates over $\mathcal{D} \times \mathcal{T}$. Visually, a simulation produced by this set of SPDE parameters is also consistent and propose a spatio-temporal diffusion process close to the original one. Because we know the process is Gaussian, we use the formula $\mathbf{Q}(x|y) = \mathbf{Q}_{xx} + \mathbf{H}^T \mathbf{R}^{-1} \mathbf{H}$, see Section 3.3, to compute the posterior variance, see Figure 7, for which the same analysis holds. It also highlights the dependency of the OI uncertainty quantification to the sampling scheme, especially here where no noise is added to the partial set of observations. On Figure 8 is also shown the time series on the same three locations than before of the GP (blue line) along the test period (15 days), the OI and corresponding standard deviation (red line), and the neural scheme estimations when the SPDE parametrization is known (orange line) or estimated (red line with associated uncertainty). Both neural scheme configurations are generally close which validates the capability of this framework to estimate jointly both state and prior parametrization. Because the neural scheme is optimized on the global MSE, its solution may deviate more or less significantly from the OI depending of the position we are looking at in domain \mathcal{D} .

Last, Figure 9 provides the scatterplot of the global MSE w.r.t the OI variational cost:

$$\mathcal{J}_{OI}(\mathbf{y}, \mathbf{x}, \hat{\boldsymbol{\theta}}) = \|\mathbf{y} - \mathbf{H}\mathbf{x}\|^2 + \mathbf{x}^T \mathbf{Q}(\hat{\boldsymbol{\theta}})\mathbf{x}$$

throughout the iteration process after training of the neural schemes. For SPDE-based prior, the initial parametrization $\boldsymbol{\theta}^{(0)}$ relates to an isotropic GP process. LSTM-based iterative solvers are all consistent with the optimal solution in terms of MSE. When the latter is used as training loss, 20 iterations is enough to reach satisfactory performance. Using the same loss for inner and outer variational cost (not shown here), see Beauchamp et al. [2022] would require more iterations to converge. Also, constraining the prior to follow the same SPDE simulation ensures to also jointly minimize the OI variational cost (asymptotic convergence of the red line to the yellow star on Figure 9) which is not the case when looking for an optimal solution within the bi-level neural optimization of prior and solver (blue line) that may lead to deviate from the original variational cost to minimize. Let note that by construction, the analytical OI solution is optimal regarding the OI variational cost: it is unbiased with minimal variance. In other words, at a given spatio-temporal location (s, t) , its variance (which is the local MSE) is minimal. In our case, we compute the global MSE

over the entire domain $\mathcal{D} \times [t_k - 2, t_k + 2]$ w.r.t the true state because we have only one single realization to compute this metrics. This is why the global MSE (see \mathcal{L}_1) of the OI may be outperformed by learning-based methods.

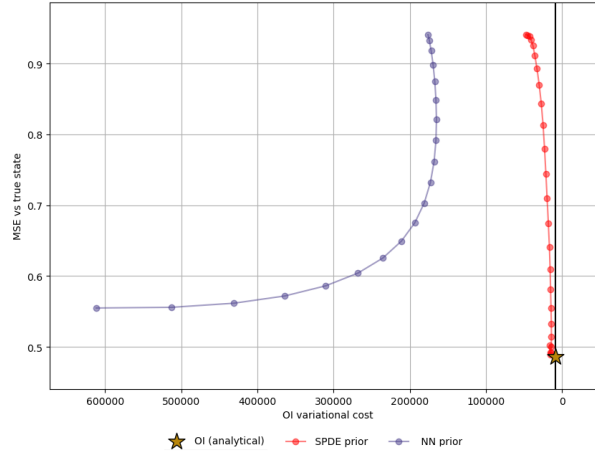


Figure 9: Optimal Interpolation derived variational cost vs Mean Squared Error (MSE) loss (a) for the gradient-based descent of the variational cost, the classical implementation of the neural scheme and its SPDE-based prior formulation. For the analytical Optimal Interpolation solution (the yellow star), there is no iterations, so a single point is displayed.

Example 7.2 Realistic SSH datasets. In this application on Sea Surface Height (SSH) spatio-temporal fields, we focus on a small part of the GULFSTREAM (see Figure 10a) mainly driven by energetic mesoscale dynamics, to illustrate how our framework may help to solve for the oversmoothing of the state-of-the-art Optimal interpolation (OI) and how the SPDE formulation of the prior is a consistent linearization of the dynamics in the data assimilation window that helps to generate ensemble members in the posterior distribution. We use an Observation System Simulation Experiment (OSSE) with the NEMO (Nucleus for European Modeling of the Ocean) model NATL60 high resolution basin-scale configuration Molines [2018].

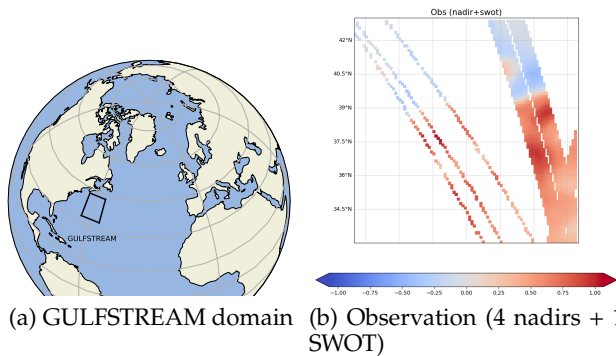


Figure 10: GULFSTREAM domain and one ($d = 0$) day accumulated along-track nadir and wide-swath SSH pseudo-observations (meters) on August 4, 2013.

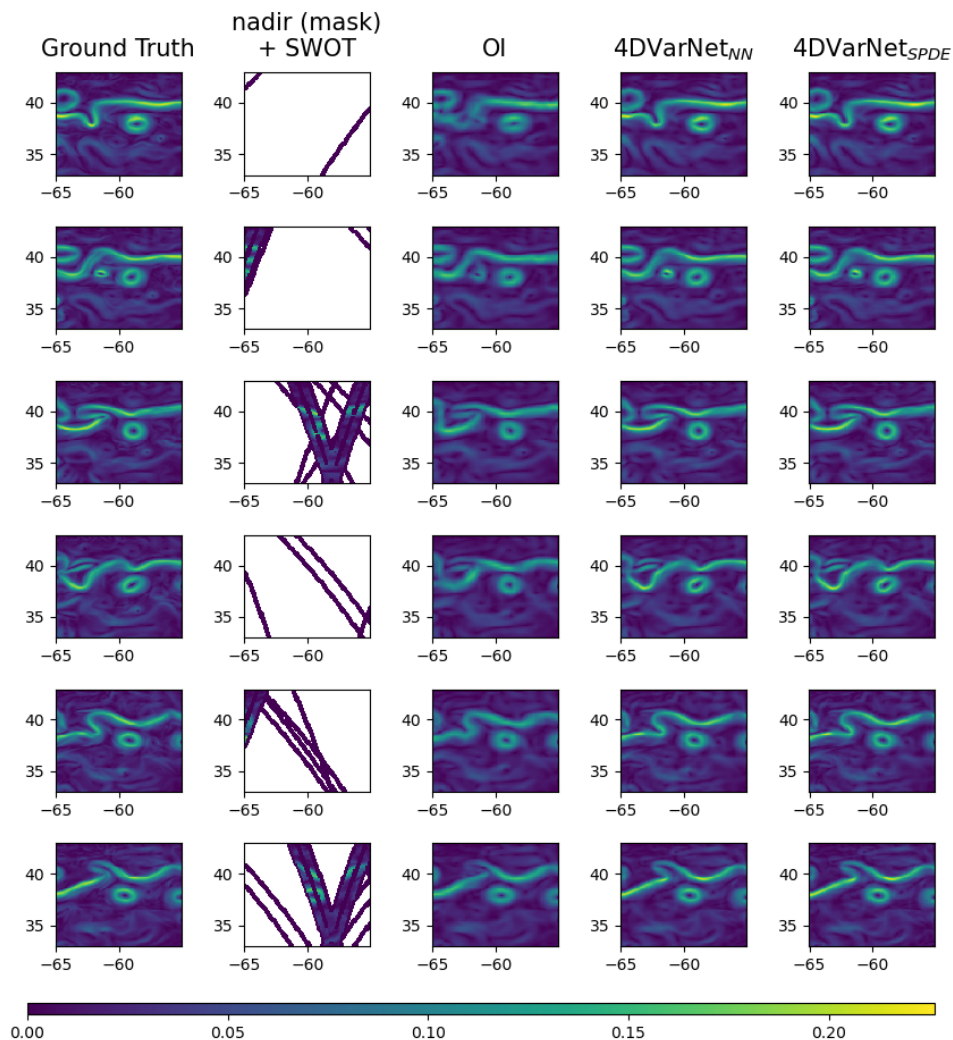


Figure 11: From left to right: SSH Gradient Ground Truth, Pseudo-observations (nadir mask and SWOT Gradient field), DUACS Optimal Interpolation, and neural variational scheme results obtained with UNet-based and SPDE-based prior operator Φ . A data assimilation window of length 5 is used

Based on this one-year long simulation, we generate pseudo along-track nadir data for the current capabilities of the observation system [Ballarotta et al., 2019] and pseudo wide-swath SWOT data in the context of the upcoming SWOT mission [Metref et al., 2020], with additional observation errors [Dufau et al., 2016, Esteban-Fernandez, 2014, Gaultier and Ubelmann, 2010]. The two types of observations may be merged, see Figure 10, to produce a one-year long daily datasets of partial and noisy observations of the idealized Ground Truth (GT). Last the DUACS operational system (CMEMS/C3S Copernicus program) provides the Optimal Interpolation baseline [Taburet et al., 2019] as daily gridded ($0.25^\circ \times 0.25^\circ$) products. All the datasets are downscaled from the original resolution of $1/60^\circ$ to $1/10^\circ$. For the training, the dataset spans from mid-February 2013 to October 2013, while the validation period refers to January 2013. All methods are tested on the test period from October 22, 2012 to December 2, 2012. We still use Adam optimizer with 100 epochs. Regarding the metrics, we use the BOOST-SWOT data challenge strategy looking at RMSE-score, and both spatial and temporel minimal scales resolved. The reader may refer to [Beauchamp et al., 2023b] for more details.

Because we aim at assessing how the use of SPDE priors in the neural architecture is relevant, we do not work directly on the SSH but on the anomaly $dx = x - \bar{x}$ between the true SSH x and its reconstruction by the DUACS system, denoted as \bar{x} . Doing so, we only focus on the reconstruction and surrogate parametrization of the small scales not caught by Optimal Interpolation. Also, the spatio-temporal correlations at such scales are significantly lower than when considering mesoscale processes as well. Then, we can reduce the data assimilation window to a reasonable length, $L = 5$ here, so that the storage of multiple (sparse) precision matrices throughout the computational graph remains possible. Moving to longer windows including mesoscale-related autocorrelations (more than 10 days) in this SPDE framework would lead to similar results, see e.g. [Febvre et al., 2022] but would require to move to matrix-free formulations, with potential existing solutions, see e.g. Pereira et al. [2022].

Last point on this experimental configuration: because the pseudo-observations are subsampled from hourly simulations but we target daily reconstructions, they are noisy due to representativity errors between the two temporal resolutions. This is not currently addressed by our framework where the observation term in the minimization cost, see Eq. 23, is only the L2-norm of the innovations. But it might be easily considered, either by using a known observation error covariance matrix \mathbf{R} or by learning one of its possible parametrization as an additional feature of the neural scheme.

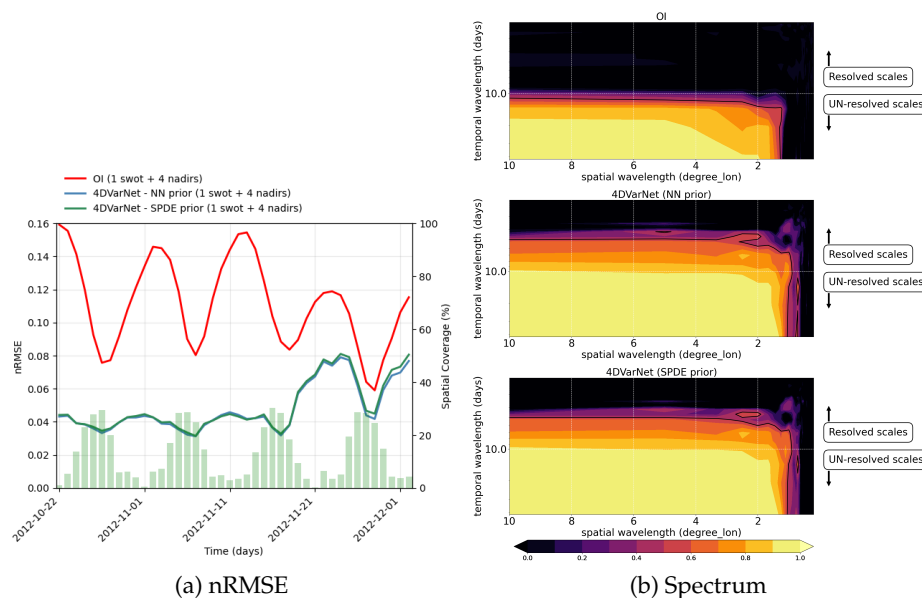


Figure 12: For DUACS Optimal Interpolation, neural solvers with UNet-based and SPDE-based prior, (a) provides their temporal performance, i.e. nRMSE time series along the BOOST-SWOT DC evaluation period ; and (b) displays their spectral performance, i.e. the PSD-based score is used to evaluate the spatio-temporal scales resolved in the GULFSTREAM domain (yellow area)

As in Example 7.1, we provide in Figure 11 the reconstructions, as the SSH gradients, obtained from DUACS OI baseline, and both neural solver formulations, the one using as prior a UNet-based parametrization, see e.g. [Beauchamp et al., 2023c] and our SPDE-based formulation. As expected and already seen in previous related studies [Beauchamp et al., 2023b,a, Fablet et al., 2021], the neural schemes improve the baseline by retrieving the dynamics along the main meander of the Gulf Stream and additional small energetic eddies. Again, there is no significant differences between the two neural formulation, which was again expected because the aim of the SPDE formulation is not to improve the mean state estimation obtained when using a neural prior operator, which is even more general, but to provide a astochastic framework for interpretability and uncertainty quantification. This is supported by Figure 12a and Figure 12b resp. showing the normalized RMSE and the space-time spectrum along the test period. The periodic improvements of the score are due to the SWOT sampling that does not provide informations every day on this Gulf Stream domain. Overall, the nRMSE is in average improved by 60% when using the neural architecture. For the spectrum, minimal spatio-temporal scales λ_x and λ_t also improve resp. by 30% and 60%. From both figures and scores provided in Table 1, we can see that the UNet formulation of prior Φ leads

to a small improvement in the reconstruction, which was expected because this is the only task optimized by the pure neural formulation. Introducing the SPDE formulation leads to optimize both reconstruction and likelihood of the parameters, which is more difficult. Though, the reconstruction performed by the latter is satisfactory enough and very close to the original solution proposed in Fablet et al. [2021].

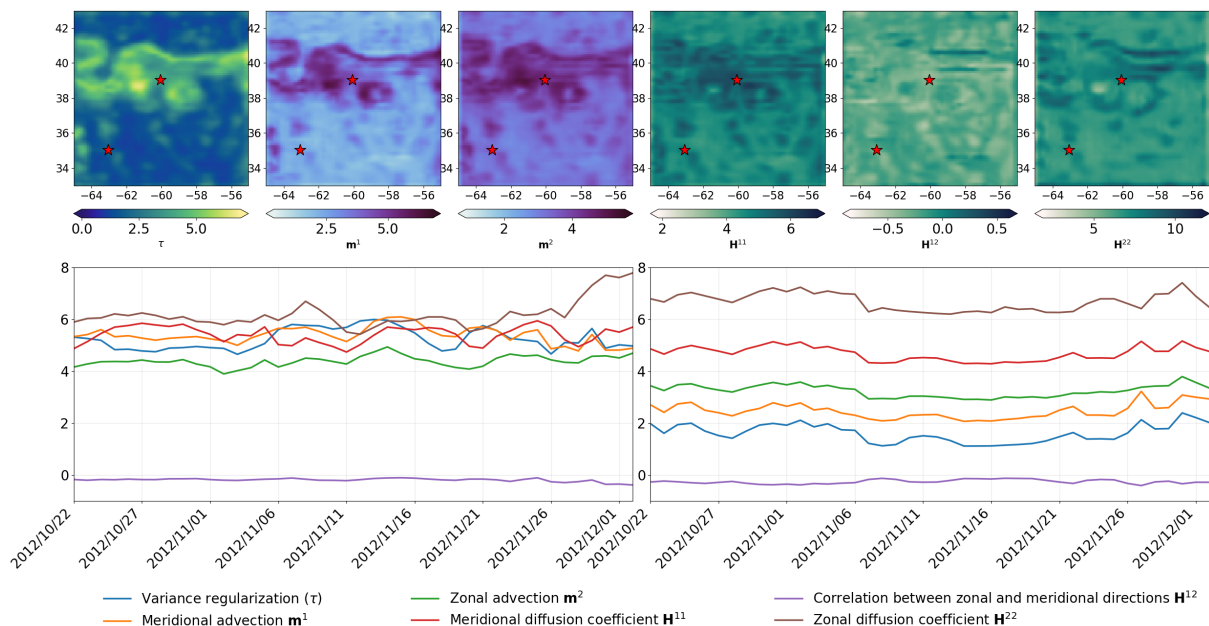


Figure 13: Parameter estimation of the SPDE prior: in the neural scheme along the 42 days test period and every 6 days. Top, from left to right: τ , \mathbf{m}^1 , \mathbf{m}^2 (advection fields), $\mathbf{H}^{1,1}$, $\mathbf{H}^{1,2}$ and $\mathbf{H}^{2,2}$ (diffusion tensor) estimated on the first day of the test period. Bottom: time series of these parameters along the test period on the two locations identified by the red stars. The first one (left) is located along the Gulf Stream meander and the second one (right) is in the less energetic left-lower part of the domain.

In this very general setup, where the equation-based dataset provide a supervised learning setting on state \mathbf{x} , but not on the SPDE parameters θ , two main questions are raised. On the first one: does the parameters retrieved by the iterative solver are interpretable? If considering Figure 13 that shows parameters τ , \mathbf{m}_1 , \mathbf{m}_2 (advection fields), \mathbf{H}_{11} , \mathbf{H}_{12} and \mathbf{H}_{22} (diffusion tensor) on the first day of the test period, they seem consistent with the anomaly field $d\mathbf{x}$ that partially encodes the SPDE parametrization, which also opens avenue for state-dependent parameters. We also show the time series along the 42 days of the test period for these parameters on two locations of the Gulf Stream domain (red stars): a first one right in the Gulf Stream meander (left time series) and a second one in the left-lower part of the domain, with less variability (right time series). Interestingly, in less energetic areas the parameters are almost perfectly correlated while in the Gulf Stream, they might behave differently. Again, as in the GP experiment, the capability of the method to catch a large range of values is demonstrated, even if the parameters are not normalized (the state is though), which is particularly the case for the diffusion tensor \mathbf{H} . Playing with both damping and variance regularization parameters provide a flexible way to handle complex GP priors with both low and high marginal variances for a given time. This is a key aspect here because the range of possible values attributed to the anomaly generally differs according to the spatio-temporal dynamics of the SSH: it is high along the main meander of the Gulf Stream and eddies not caught up by the OI, and lower elsewhere. This is also supported by generating non-conditional simulations based on these parameters and comparing it to the ground truth anomalies: Figure 14 shows five spatio-temporal simulations of the anomaly along the data assimilation window for the tenth day of the test period, when using the SPDE parametrization provided by the neural solver. The spatio-temporal fields are clearly coherent with the original simulation which also makes the link between our approach and generative modeling. The average of a large number of simulations would be a zero state, while its covariance relates to the model error matrix used in equation-based DA to perturb the members in ensemble methods. Let note that contrary to the GP experiment, no prior is accessible for the initialization of the SPDE parameters in the iterative solution: all are set to zeros, except κ and τ that are set to 0.1.

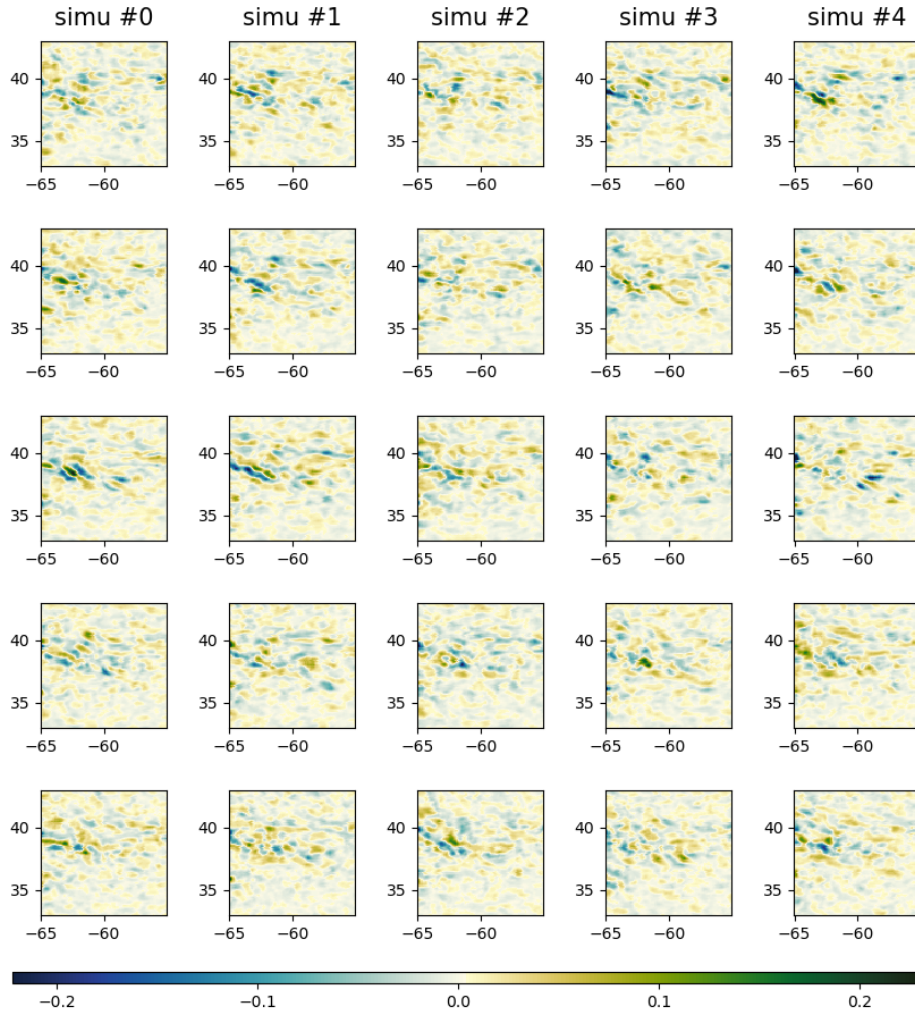


Figure 14: From left to right, five non-conditional simulations of the anomaly dx

| | $\mu(\text{RMSE})$ | $\sigma(\text{RMSE})$ | λ_x (degree) | λ_t (days) |
|---|--------------------|-----------------------|----------------------|--------------------|
| OI (1 swot + 4 nadirs) | 0.92 | 0.02 | 1.22 | 11.06 |
| 4DVarNet - NN prior (1 swot + 4 nadirs) | 0.97 | 0.01 | 0.89 | 4.40 |
| 4DVarNet - SPDE prior (1 swot + 4 nadirs) | 0.96 | 0.01 | 0.90 | 5.03 |

Table 1: Scores

The second question is: does this approach, SPDE-based generation of members, followed by their conditioning with observations, is efficient to estimate the posterior pdf $p_{x|y}$? Figure 15 shows the estimated posterior standard deviations, when using the Gaussian equation, see Example 7.1 and Section 3.3, or the empirical posterior standard deviations computed from 250 members, again for the tenth day of the test period. They are given together with their associated reconstruction error $x - x^*$. All the three are displayed along the data assimilation window for time 0, 2 and 4. It is clear how the posterior standard deviation produced by the OI equations only depends on the tracks of satellite altimetry (nadirs and SWOT) and the prior covariance $\mathbf{P}(\theta^*)$. It does not seem relevant to approximate the reconstruction error given in right panels. Looking at the estimated standard deviation produced by the ensemble of neural variational reconstructions, they are less dependent of the observations: we can still see the observation

mask as blurry areas in the middle panels but the standard deviations is more continuous and flow dependent. The correlation with the absolute error is good, meaning that this posterior standard deviation produced by the ensemble is consistent: when low, the average reconstruction is generally very good.

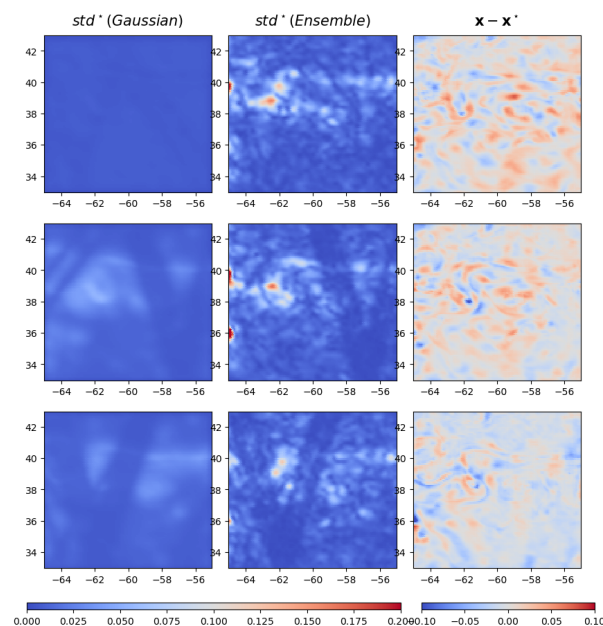


Figure 15: From left to right: estimated posterior standard deviations (gaussian hypothesis of the posterior and ensemble-based neural scheme) and corresponding reconstruction error at the beginning, center and end of the assimilation window $time = 0, 2, 4$ (from top to bottom)

In Appendix D, we provide complementary details regarding how the proposed SPDE parametrization of the prior may be physically sounded for this problem of SSH reconstruction, by connecting the simplified quasi-geostrophic (QG) theory with potential SPDE additional formulations.

8 Conclusion

We explore a new neural architecture to tackle the reconstruction inverse problem of a dynamical process from partial and potentially noisy observations. We provide a joint end-to-end learning scheme of both stochastic prior models and solvers. The idea is to optimize in the same time the state and the stochastic parametrization of the prior so that we minimize the mean squared error between the reconstruction and the true states, while we are also able to provide uncertainty quantification of the mean state reconstruction, either analytically in the gaussian case, or ensemble-derived in the more general configuration.

In our work, we draw from recent advances in geostatistical simulations of SPDE-based Gaussian Processes to provide a flexible trainable prior embedded in a neural architecture backbone on variational data assimilation. The SPDE parameters are added as latent variables in an augmented state the trainable solver has to reconstruct. A bi-level optimization scheme is used to optimize in the same time:

- the inner variational cost derived from OI-based formulations, which depends on state x , observations y and SPDE parameters θ and,
- the outer training loss function of the neural architecture, which drives the optimization of the LSTM-based residual solver parameters θ leading to the reconstruction of the augmented state.

The first application of the framework on a diffusion-based GP showed that it reaches the same performance, in terms of MSE w.r.t the ground truth, observed when using a neural-based prior in the classic implementation fo the neural scheme [Fablet et al., 2020], which asymptotically converges towards the

optimal solution. In addition, the posterior variance of the mean state derived from the SPDE parameters is close to the true variance of the Optimal Interpolation, which demonstrates the potentiality of the proposed scheme to handle uncertainty quantifications. Indeed, if we showed that retrieving the original set of SPDE parameters might be difficult, the local minimum found after the training process leads to a parametrization with high likelihood, similar diffusion-based spatial patterns and spatio-temporal covariances structures. Though not always physically explainable, the SPDE prior formulation still helps to interpret the dynamical process in terms of statistical properties.

In a more general setup, we also present an application on Sea Surface Height dynamics based on Observation System Simulation Experiment (OSSE), for which the ground truth is given by a state-of-the-art ocean model and pseudo-observations are generated by a realistic satellite subsampling of the ground truth. In this case, the process is not linear and the gaussian framework do not apply. Then, the idea is to use the GP linear SPDE formulation as a surrogate model to linearize the prior dynamics along the data assimilation window. It provides an efficient way for fast sampling of a huge set of members in the prior distribution within a few minutes. Based on the neural solver, able to handle non-linear and non-gaussian dynamics based on its supervised training, the conditioning of these simulations leads to the estimation of the posterior distribution. The preliminary conclusions made on the GP experiment holds for the reconstruction of the mean state, i.e. no significant differences observed when using a trainable neural prior. The key aspect of the framework is here revealed by the SPDE parametrization, which is fully non-stationary in space and time, and allow for online estimation after training for any new set of input observations, in contrast with other approaches in most of the spatial statistics literature which requires offline new parameter inference. We showed that the prior parametrization is both statistically consistent with the original ground truth used in the training and physically sounded with similar patterns observed in the advection components estimated by both our framework and the QG theory. Comparing the posterior pdf retrieved from the ensemble members, higher variances are observed in areas of high reconstruction errors which is a good indicator of the framework capability to quantify realistic uncertainties. Additional applications would be necessary on real datasets to complement these preliminary conclusions.

Regarding the potential extensions of this methodology, it is important to understand that such an SPDE parametrization of the prior term is a way of going to generative modelling, as it is called in the machine learning community. In our case, the SPDE is linear and already provide an efficient way to produce fast, large and realistic ensembles. Promising avenues would be to draw from the existing link between diffusion models and SDE to enrich our framework, provide stochastic non-linear priors and see if and how it helps to improve again the results obtained in this work. Also, we made the choice to model the prior with a linear SPDE before conditioning it with our neural solver. A direct use of the SPDE formulation for the posterior would have been possible, but restrictive to GP reconstructions which is in most cases rather limited. Back to the non-linear neural diffusion operators, an other way of addressing the problem would be to directly optimize the sampling in the posterior pdf.

References

- B. D. Anderson. Reverse-time diffusion equation models. *Stochastic Processes and their Applications*, 12(3): 313–326, May 1982. URL <https://ideas.repec.org/a/eee/spapps/v12y1982i3p313-326.html>.
- M. Andrychowicz, M. Denil, S. Gomez, M. W. Hoffman, D. Pfau, T. Schaul, B. Shillingford, and N. De Freitas. Learning to learn by gradient descent by gradient descent. In *Advances in neural information processing systems*, pages 3981–3989, 2016.
- L. Arras, J. Arjona-Medina, M. Widrich, G. Montavon, M. Gillhofer, K.-R. Müller, S. Hochreiter, and W. Samek. Explaining and interpreting lstms. *Lecture Notes in Computer Science*, pages 211–238, 2019. ISSN 1611-3349. doi: 10.1007/978-3-030-28954-6_11. URL http://dx.doi.org/10.1007/978-3-030-28954-6_11.
- M. Asch, M. Bocquet, and M. Nodet. *Data Assimilation. Fundamentals of Algorithms*. Society for Industrial and Applied Mathematics, Dec. 2016. ISBN 978-1-61197-453-9. doi: 10.1137/1.9781611974546. URL <https://doi.org/10.1137/1.9781611974546>.
- M. Ballarotta, C. Ubelmann, M.-I. Pujol, G. Taburet, F. Fournier, J.-F. Legeais, Y. Faugère, A. Delepouille, D. Chelton, G. Dibaroure, and N. Picot. On the resolutions of ocean altimetry maps. *Ocean Science*, 15(4):1091–1109, 2019. doi: 10.5194/os-15-1091-2019. URL <https://www.ocean-sci.net/15/1091/2019/>.
- M. Beauchamp, J. Thompson, H. Georgenthum, Q. Febvre, and R. Fablet. Learning neural optimal interpolation models and solvers, 2022. URL <https://arxiv.org/abs/2211.07209>.

- M. Beauchamp, Q. Febvre, and R. Fablet. Ensemble-based 4dvarnet uncertainty quantification for the reconstruction of sea surface height dynamics. *Environmental Data Science*, 2:e18, 2023a. doi: 10.1017/eds.2023.19.
- M. Beauchamp, Q. Febvre, H. Georgenthum, and R. Fablet. 4dvarnet-ssh: end-to-end learning of variational interpolation schemes for nadir and wide-swath satellite altimetry. *Geoscientific Model Development*, 16(8): 2119–2147, 2023b. doi: 10.5194/gmd-16-2119-2023. URL <https://gmd.copernicus.org/articles/16/2119/2023/>.
- M. Beauchamp, Q. Febvre, J. Thompson, H. Georgenthum, and R. Fablet. Learning neural optimal interpolation models and solvers. In J. Mikyška, C. de Mulatier, M. Paszynski, V. V. Krzhizhanovskaya, J. J. Dongarra, and P. M. Soot, editors, *Computational Science – ICCS 2023*, pages 367–381, Cham, 2023c. Springer Nature Switzerland. ISBN 978-3-031-36027-5.
- D. Bolin and J. Wallin. Spatially adaptive covariance tapering. *Spatial Statistics*, 18:163–178, 2016. ISSN 2211-6753. doi: <https://doi.org/10.1016/j.spasta.2016.03.003>. URL <https://www.sciencedirect.com/science/article/pii/S2211675316000245>. Spatial Statistics Avignon: Emerging Patterns.
- M. Cameletti, F. Lindgren, D. Simpson, and H. Rue. Spatio-temporal modeling of particulate matter concentration through the SPDE approach. *ASTA Advances in Statistical Analysis*, pages 1–23, 2013. URL <http://link.springer.com/article/10.1007/s10182-012-0196-3>.
- A. Carrassi, M. Bocquet, L. Bertino, and G. Evensen. Data assimilation in the geosciences: An overview of methods, issues, and perspectives. *WIREs Climate Change*, 9(5):e535, 2018. doi: <https://doi.org/10.1002/wcc.535>. URL <https://onlinelibrary.wiley.com/doi/abs/10.1002/wcc.535>.
- Y. Chen, T. Davis, W. Hager, and S. Rajamanickam. Algorithm 887: Cholmod, supernodal sparse cholesky factorization and update/downdate. *ACM Trans. Math. Softw.*, 35, 01 2008.
- J. Chilès and P. Delfiner. *Geostatistics : modeling spatial uncertainty*. Wiley, New-York, second edition, 2012.
- J.-P. Chilès and N. Desassis. *Fifty Years of Kriging*, pages 589–612. Springer International Publishing, Cham, 2018. ISBN 978-3-319-78999-6. doi: 10.1007/978-3-319-78999-6_29. URL https://doi.org/10.1007/978-3-319-78999-6_29.
- L. Clarotto, D. Allard, T. Romary, and N. Desassis. The spde approach for spatio-temporal datasets with advection and diffusion, 2022. URL <https://arxiv.org/abs/2208.14015>.
- F. Counillon and L. Bertino. Ensemble optimal interpolation: multivariate properties in the gulf of mexico. *Tellus A*, 61(2):296–308, 2009. doi: <https://doi.org/10.1111/j.1600-0870.2008.00383.x>. URL <https://onlinelibrary.wiley.com/doi/abs/10.1111/j.1600-0870.2008.00383.x>.
- N. Cressie and C. Wikle. *Statistics for Spatio-Temporal Data*. John Wiley & Sons, 2015. ISBN 978-1-119-24304-5.
- L. Dinh, J. Sohl-Dickstein, and S. Bengio. Density estimation using real nvp, 2017.
- C. Dufau, M. Orsztynowicz, G. Dibarboure, R. Morrow, and P.-Y. Le Traon. Mesoscale resolution capability of altimetry: Present and future. *Journal of Geophysical Research: Oceans*, 121(7):4910–4927, 2016. doi: 10.1002/2015JC010904. URL <https://agupubs.onlinelibrary.wiley.com/doi/abs/10.1002/2015JC010904>.
- R. E. Ewing and H. Wang. A summary of numerical methods for time-dependent advection-dominated partial differential equations. *Journal of Computational and Applied Mathematics*, 128(1):423–445, 2001. ISSN 0377-0427. doi: [https://doi.org/10.1016/S0377-0427\(00\)00522-7](https://doi.org/10.1016/S0377-0427(00)00522-7). URL <https://www.sciencedirect.com/science/article/pii/S0377042700005227>. Numerical Analysis 2000. Vol. VII: Partial Differential Equations.
- D. Esteban-Fernandez. Swot project mission performance and error budget document. Technical report, JPL, NASA, 2014.
- G. Evensen. *Data Assimilation*. Springer Berlin Heidelberg, Berlin, Heidelberg, 2009. ISBN 9783642037108 9783642037115. URL <http://link.springer.com/10.1007/978-3-642-03711-5>.
- G. Evensen, F. C. Vossepoel, and P. J. van Leeuwen. *Data Assimilation Fundamentals*. Springer Textbooks in Earth Sciences, Geography and Environment (STEGER). Springer Cham, 2022. ISBN 978-3-030-96708-6. doi: 10.1007/978-3-030-96709-3. URL <https://doi.org/10.1007/978-3-030-96709-3>.
- R. Fablet, L. Drumetz, and F. Rousseau. Joint learning of variational representations and solvers for inverse problems with partially-observed data. *arXiv:2006.03653 [physics]*, 2020. URL <https://arxiv.org/abs/2006.03653>. arXiv:2006.03653.

- R. Fablet, B. Chapron, L. Drumetz, E. Mémin, O. Pannekoek, and F. Rousseau. Learning variational data assimilation models and solvers. *Journal of Advances in Modeling Earth Systems*, 13(10):e2021MS002572, 2021. doi: <https://doi.org/10.1029/2021MS002572>. URL <https://agupubs.onlinelibrary.wiley.com/doi/abs/10.1029/2021MS002572>. e2021MS002572 2021MS002572.
- Q. Febvre, R. Fablet, J. L. Sommer, and C. Ubelmann. Joint calibration and mapping of satellite altimetry data using trainable variational models. In *ICASSP 2022 - 2022 IEEE International Conference on Acoustics, Speech and Signal Processing (ICASSP)*, pages 1536–1540, 2022. doi: 10.1109/ICASSP43922.2022.9746889.
- B. A. Finlayson. *Numerical Methods for Problems with Moving Fronts*. Ravenna Park Publishing, Seattle, 1992.
- G.-A. Fuglstad, F. Lindgren, D. Simpson, and H. Rue. Exploring a new class of non-stationary spatial gaussian random fields with varying local anisotropy. *Statistica Sinica*, 25(1):115–133, 2015a. ISSN 1017-0405. doi: 10.5705/ss.2013.106w.
- G.-A. Fuglstad, D. Simpson, F. Lindgren, and H. Rue. Does non-stationary spatial data always require non-stationary random fields? *Spatial Statistics*, 14:505–531, 2015b. ISSN 2211-6753. doi: <https://doi.org/10.1016/j.spasta.2015.10.001>. URL <https://www.sciencedirect.com/science/article/pii/S2211675315000780>.
- G.-A. Fuglstad, D. Simpson, F. Lindgren, and H. Rue. Does non-stationary spatial data always require non-stationary random fields? *Spatial Statistics*, 14:505 – 531, 2015c. ISSN 2211-6753. doi: <https://doi.org/10.1016/j.spasta.2015.10.001>. URL <http://www.sciencedirect.com/science/article/pii/S2211675315000780>.
- R. Furrer, M. G. Genton, and D. Nychka. Covariance tapering for interpolation of large spatial datasets. *Journal of Computational and Graphical Statistics*, 15(3):502–523, 2006. ISSN 10618600. URL <http://www.jstor.org/stable/27594195>.
- L. Gaultier and C. Ubelmann. Swot simulator documentation. Technical report, JPL, NASA, 2010.
- M. G. Genton. Classes of kernels for machine learning: A statistics perspective. *J. Mach. Learn. Res.*, 2: 299–312, mar 2002. ISSN 1532-4435.
- I. J. Goodfellow, J. Pouget-Abadie, M. Mirza, B. Xu, D. Warde-Farley, S. Ozair, A. Courville, and Y. Bengio. Generative adversarial nets. In *Proceedings of the 27th International Conference on Neural Information Processing Systems - Volume 2, NIPS'14*, page 2672–2680, Cambridge, MA, USA, 2014. MIT Press.
- U. Grenander and M. I. Miller. Representations of knowledge in complex systems. *Journal of the Royal Statistical Society. Series B (Methodological)*, 56(4):549–603, 1994. ISSN 00359246. URL <http://www.jstor.org/stable/2346184>.
- A. Grigorievskiy, N. D. Lawrence, and S. Särkkä. Parallelizable sparse inverse formulation gaussian processes (spingp). *2017 IEEE 27th International Workshop on Machine Learning for Signal Processing (MLSP)*, pages 1–6, 2016.
- J. Ho, A. Jain, and P. Abbeel. Denoising diffusion probabilistic models, 2020.
- D. P. Kingma and M. Welling. Auto-encoding variational bayes, 2022.
- H. Lewy, K. Friedrichs, and R. Courant. Über die partiellen differenzgleichungen der mathematischen physik. *Mathematische Annalen*, 100:32–74, 1928. URL <http://eudml.org/doc/159283>.
- F. Lindgren, H. Rue, and J. Lindström. An explicit link between gaussian fields and gaussian markov random fields: the stochastic partial differential equation approach. *Journal of the Royal Statistical Society: Series B (Statistical Methodology)*, 73(4):423–498, 2011. doi: 10.1111/j.1467-9868.2011.00777.x. URL <https://rss.onlinelibrary.wiley.com/doi/abs/10.1111/j.1467-9868.2011.00777.x>.
- L. Menut, B. Bessagnet, R. Briant, A. Cholakian, F. Couvidat, S. Mailler, R. Pennel, G. Siour, P. Tuccella, S. Turquety, and M. Valari. The chimere v2020r1 online chemistry-transport model. *Geoscientific Model Development*, 14(11):6781–6811, 2021. doi: 10.5194/gmd-14-6781-2021. URL <https://gmd.copernicus.org/articles/14/6781/2021/>.
- S. Metref, E. Cosme, F. Le Guillou, J. Le Sommer, J.-M. Brankart, and J. Verron. Wide-swath altimetric satellite data assimilation with correlated-error reduction. *Frontiers in Marine Science*, 6:822, 2020. ISSN 2296-7745. doi: 10.3389/fmars.2019.00822. URL <https://www.frontiersin.org/article/10.3389/fmars.2019.00822>.
- J.-M. Molines. meom-configurations/NATL60-CJM165: NATL60 code used for CJM165 experiment, Mar. 2018. URL <https://zenodo.org/record/1210116#.XDpmc89Khp8>.

- A. Paszke, S. Gross, S. Chintala, G. Chanan, E. Yang, Z. DeVito, Z. Lin, A. Desmaison, L. Antiga, and A. Lerer. Automatic differentiation in pytorch. 2017.
- M. Pereira, N. Desassis, and D. Allard. Geostatistics for large datasets on riemannian manifolds: A matrix-free approach. *Journal of Data Science*, 20(4):512–532, 2022. ISSN 1680-743X. doi: 10.6339/22-JDS1075.
- H. S. Price, R. S. Varga, and J. E. Warren. Applications of oscillation matrices to diequations. *J. Math. Phys*, 45, 1966.
- H. Rue and L. Held. *Gaussian markov random fields: Theory and applications*. 01 2005.
- J. J. Ruiz, M. Pulido, and T. Miyoshi. Estimating model parameters with ensemble-based data assimilation: A review. *Journal of the Meteorological Society of Japan. Ser. II*, 91(2):79–99, 2013.
- S. Särkka and J. Hartikainen. Infinite-dimensional kalman filtering approach to spatio-temporal gaussian process regression. In N. D. Lawrence and M. Girolami, editors, *Proceedings of the Fifteenth International Conference on Artificial Intelligence and Statistics*, volume 22 of *Proceedings of Machine Learning Research*, pages 993–1001, La Palma, Canary Islands, 21–23 Apr 2012. PMLR. URL <https://proceedings.mlr.press/v22/sarkka12.html>.
- S. Särkka, A. Solin, and J. Hartikainen. Spatiotemporal learning via infinite-dimensional bayesian filtering and smoothing: A look at gaussian process regression through kalman filtering. *IEEE Signal Processing Magazine*, 30(4):51–61, 2013. doi: 10.1109/MSP.2013.2246292.
- M. Seeger, A. Hetzel, Z. Dai, E. Meissner, and N. D. Lawrence. Auto-differentiating linear algebra, 2019.
- F. Sigrist, H. R. Künsch, and W. A. Stahel. Stochastic partial differential equation based modelling of large space–time data sets. *Journal of the Royal Statistical Society: Series B (Statistical Methodology)*, 77(1):3–33, 2015. doi: <https://doi.org/10.1111/rssb.12061>. URL <https://rss.onlinelibrary.wiley.com/doi/abs/10.1111/rssb.12061>.
- J. Sohl-Dickstein, E. A. Weiss, N. Maheswaranathan, and S. Ganguli. Deep unsupervised learning using nonequilibrium thermodynamics, 2015.
- J. C. Strikwerda. *Finite Difference Schemes and Partial Differential Equations (Wadsworth & Brooks/Cole Mathematics Series)*. Wadsworth & BrooksCole Advanced Books & Software, Pacific Grove, 1989.
- G. Taburet, A. Sanchez-Roman, M. Ballarotta, M.-I. Pujol, J.-F. Legeais, F. Fournier, Y. Faugere, and G. Dibaroure. DUACS DT2018: 25 years of reprocessed sea level altimetry products. 15(5):1207–1224, 2019. ISSN 1812-0784. doi: <https://doi.org/10.5194/os-15-1207-2019>. URL <https://www.ocean-sci.net/15/1207/2019/>. Publisher: Copernicus GmbH.
- P. Tandeo, P. Ailliot, J. Ruiz, A. Hannart, B. Chapron, A. Cuzol, V. Monbet, R. Easton, and R. Fablet. Combining Analog Method and Ensemble Data Assimilation: Application to the Lorenz-63 Chaotic System. In V. Lakshmanan, E. Gilleland, A. McGovern, and M. Tingley, editors, *Machine Learning and Data Mining Approaches to Climate Science*, pages 3–12. Springer, 2015.
- P.-Y. Traon, F. Nadal, and N. Ducet. An improved mapping method of multisatellite altimeter data. *Journal of Atmospheric and Oceanic Technology*, 15(2):522–534, 1998. doi: 10.1175/1520-0426(1998)015<0522:AIMMOM>2.0.CO;2. URL https://journals.ametsoc.org/view/journals/atot/15/2/1520-0426_1998_015_0522_aimmom_2_0_co_2.xml.
- C. Ubelmann, P. Klein, and L.-L. Fu. Dynamic Interpolation of Sea Surface Height and Potential Applications for Future High-Resolution Altimetry Mapping. *Journal of Atmospheric and Oceanic Technology*, 32(1):177–184, Oct. 2014. ISSN 0739-0572. doi: 10.1175/JTECH-D-14-00152.1. URL <http://journals.ametsoc.org/doi/abs/10.1175/JTECH-D-14-00152.1>.
- P. Virtanen, R. Gommers, T. E. Oliphant, M. Haberland, T. Reddy, D. Cournapeau, E. Burovski, P. Peterson, W. Weckesser, J. Bright, S. J. van der Walt, M. Brett, J. Wilson, K. J. Millman, N. Mayorov, A. R. J. Nelson, E. Jones, R. Kern, E. Larson, C. J. Carey, Í. Polat, Y. Feng, E. W. Moore, J. VanderPlas, D. Laxalde, J. Perktold, R. Cimrman, I. Henriksen, E. A. Quintero, C. R. Harris, A. M. Archibald, A. H. Ribeiro, F. Pedregosa, P. van Mulbregt, and SciPy 1.0 Contributors. SciPy 1.0: Fundamental Algorithms for Scientific Computing in Python. *Nature Methods*, 17:261–272, 2020. doi: 10.1038/s41592-019-0686-2.
- H. Wackernagel. *Multivariate Geostatistics. An Introduction with Applications*. Springer-Verlag Berlin Heidelberg, New York, 2003. doi: 10.1007/978-3-662-05294-5. ISBN 978-3-540-44142-7.
- P. Whittle. On stationary processes in the plane. *Biometrika*, 41(3-4):434–449, 1953. doi: 10.1093/biomet/41.3-4.434. URL <http://biomet.oxfordjournals.org/content/41/3-4/434.short>.

A Precision on the covariance matrices involved in the SPDE model

In the spatio-temporal OI formulation, we define an SPDE-based prior $\mathbf{x} = \{\mathbf{x}_0, \dots, \mathbf{x}_{Ldt}\}$ with covariance matrices between two consecutive time steps being defined according to the implicit Euler scheme, see Eq. (14):

$$\mathbf{P}_{t+dt,t} = \text{Cov}\{\mathbf{x}_{t+dt}, \mathbf{x}_t\} = \text{Cov}\{\mathbf{M}_{t+dt}\mathbf{x}_t + \mathbf{T}_{t+dt}\mathbf{z}_{t+dt}, \mathbf{x}_t\} = \mathbf{M}_{t+dt}\mathbf{P}_{t,t}$$

This leads to both forward and backward iterative covariance recursions:

$$\mathbf{P}_{t+kdt,t} = \prod_{l=k}^1 \mathbf{M}_{t+lkd} \mathbf{P}_{t,t}$$

$$\mathbf{P}_{t,t+kdt} = \mathbf{P}_{t,t} \prod_{l=1}^k \mathbf{M}_{t+lkd}$$

Let note that if operator \mathbf{B} does not depend on time, then neither \mathbf{P} , then the forward and backward recursions simplifies to:

$$\mathbf{P}_{t+kdt,t} = \mathbf{M}^k \mathbf{P}$$

$$\mathbf{P}_{t,t+kdt} = \mathbf{P} \mathbf{M}^k$$

Also, the SPDE evolution model for prior \mathbf{x} gives the evolution formulation of the covariance from time t to $t + dt$:

$$\mathbf{P}_{t+dt} = \mathbf{M}_{t+dt} \left[\mathbf{P}_t + dt \boldsymbol{\tau}_t \mathbf{Q}_s^{-1} \boldsymbol{\tau}_t^\top \right] \mathbf{M}_{t+dt}^\top \quad (35)$$

where the term $dt \boldsymbol{\tau}_t \mathbf{Q}_s^{-1} \boldsymbol{\tau}_t^\top$ simplifies to $\tau^2 dt \mathbf{Q}_s^{-1}$ in the case $\boldsymbol{\tau}_t = \boldsymbol{\tau}$ is a scalar constant in space and time.

B Finite difference schemes for SPDE

In this work, we propose to use the Euler implicit scheme as a discretization method for the stochastic PDEs. We need to define the discretized version of several differential operators on the 2D regular grid, namely:

B.1 Discretization of the spatial differential operators

$$\begin{aligned}
 \Delta \mathbf{x}_{i,j} &= \frac{\partial^2 \mathbf{x}}{\partial x^2}_{i,j} + \frac{\partial^2 \mathbf{x}}{\partial y^2}_{i,j} \\
 &= \frac{\partial}{\partial x} \left(\frac{\partial \mathbf{x}}{\partial x} \right)_{i,j} + \frac{\partial}{\partial y} \left(\frac{\partial \mathbf{x}}{\partial y} \right)_{i,j} \\
 &= \frac{\partial}{\partial x} \left(\frac{\mathbf{x}_{i+1,j} - \mathbf{x}_{i-1,j}}{2dx} \right) + \frac{\partial}{\partial y} \left(\frac{\mathbf{x}_{i,j+1} - \mathbf{x}_{i,j-1}}{2dy} \right) \\
 &= \left(\frac{\mathbf{x}_{i+1,j}}{dx^2} - \frac{\mathbf{x}_{i,j}}{dx^2} \right) - \left(\frac{\mathbf{x}_{i,j}}{dx^2} - \frac{\mathbf{x}_{i-1,j}}{dx^2} \right) \\
 &\quad + \left(\frac{\mathbf{x}_{i,j+1}}{dy^2} - \frac{\mathbf{x}_{i,j}}{dy^2} \right) - \left(\frac{\mathbf{x}_{i,j}}{dy^2} - \frac{\mathbf{x}_{i,j-1}}{dy^2} \right) \\
 &= \frac{\mathbf{x}_{i+1,j} - 2\mathbf{x}_{i,j} + \mathbf{x}_{i-1,j}}{dx^2} + \frac{\mathbf{x}_{i,j+1} - 2\mathbf{x}_{i,j} + \mathbf{x}_{i,j-1}}{dy^2}
 \end{aligned} \tag{36a}$$

$$\begin{aligned}
 \nabla \mathbf{H} \cdot \nabla \mathbf{x}_{i,j} &= \left(\mathbf{H}^{1,1} \frac{\partial}{\partial x^2} + \mathbf{H}^{1,2} \frac{\partial}{\partial x \partial y} + \mathbf{H}^{2,1} \frac{\partial}{\partial x \partial y} + \mathbf{H}^{2,2} \frac{\partial}{\partial y^2} \right) \mathbf{x}_{i,j} \\
 &= \mathbf{H}^{1,1} \frac{\mathbf{x}_{i+1,j} - 2\mathbf{x}_{i,j} + \mathbf{x}_{i-1,j}}{dx^2} \\
 &\quad + \mathbf{H}^{2,2} \frac{\mathbf{x}_{i,j+1} - 2\mathbf{x}_{i,j} + \mathbf{x}_{i,j-1}}{dy^2} \\
 &\quad + \mathbf{H}^{1,2} \frac{\mathbf{x}_{i+1,j+1} - \mathbf{x}_{i+1,j-1} - \mathbf{x}_{i-1,j+1} + \mathbf{x}_{i-1,j-1}}{4dxdy} \\
 &\quad + \mathbf{H}^{2,1} \frac{\mathbf{x}_{i+1,j+1} - \mathbf{x}_{i-1,j+1} - \mathbf{x}_{i+1,j-1} + \mathbf{x}_{i-1,j-1}}{4dxdy} \\
 &= \mathbf{H}^{1,1} \frac{\mathbf{x}_{i+1,j} - 2\mathbf{x}_{i,j} + \mathbf{x}_{i-1,j}}{dx^2} \\
 &\quad + \mathbf{H}^{2,2} \frac{\mathbf{x}_{i,j+1} - 2\mathbf{x}_{i,j} + \mathbf{x}_{i,j-1}}{dy^2} \\
 &\quad + \mathbf{H}^{1,2} \frac{\mathbf{x}_{i+1,j+1} - \mathbf{x}_{i+1,j-1} - \mathbf{x}_{i-1,j+1} + \mathbf{x}_{i-1,j-1}}{2dxdy}
 \end{aligned} \tag{36b}$$

$$\begin{aligned}
 \mathbf{m} \cdot \nabla \mathbf{x}_{i,j} &= \mathbf{m}^1 \frac{\partial}{\partial x} \mathbf{x}_{i,j} + \mathbf{m}^2 \frac{\partial}{\partial y} \mathbf{x}_{i,j} \\
 &= \mathbf{m}^1 \frac{\mathbf{x}_{i+1,j} - \mathbf{x}_{i-1,j}}{2dx} + \mathbf{m}^2 \frac{\mathbf{x}_{i,j+1} - \mathbf{x}_{i,j-1}}{2dy}
 \end{aligned} \tag{36c}$$

B.2 Upwind schemes for advection-dominated SPDE

With such an advection-diffusion framework detailed in Section 4, it is known that the solution to the space-centered scheme does not oscillate only when the Peclet number is lower than 2 and the Courant–Friedrichs–Lewy condition (CFL) condition $Cr = dt (\mathbf{m}^1/dx + \mathbf{m}^2/dy) \leq 1$ is satisfied [Lewy et al., 1928, Price et al., 1966]. For unsatisfied Peclet conditions, damped oscillations occur with nonreal

eigenvalues [Finlayson, 1992, Price et al., 1966], while in the limiting case of pure advection $\mathbf{H} \rightarrow \mathbf{0}$, such a scheme would be unconditionally unstable [Finlayson, 1992, Strikwerda, 1989]. Because the velocity fields are allowed to vary in space and time, the CFL number is different at each discrete space-time location (i, j, t) . A necessary condition for convergence is that the CFL condition be satisfied at each point location, the velocity and diffusion parameters being unknown, we have to choose the timestep dt small enough so that the maximum CFL number (observed in space at each time step) satisfies the CFL condition. Again, because the velocity field is trained, it may happen that the CFL condition is not satisfied if the latter is more and more dominant during the training. A simple way of counteracting this problem is to use an activation function on the two velocity components by clipping their maximum value.

One way of addressing this problem of stabilities in FDM when the advection term is predominant over the diffusion relates to the class of upwind schemes (UFDM). It is used to numerically simulate more properly the direction of propagation of the state in a flow field. The first order upwind FDM uses a one-sided finite difference in the upstream direction to approximate the advection term in the transport SPDE. The spatial accuracy of the first-order upwind scheme can be improved by choosing a more accurate finite difference stencil for the approximation of spatial derivative. Let note that UFDM scheme for SPDE eliminates the nonphysical oscillations in the space-centered scheme and generate stable solutions even for very complicated flows.

B.2.1 First-order upwind scheme (UFDM1)

Instead of using centered differences:

$$\left(\frac{\partial \mathbf{x}}{\partial x}\right)_{i,j} = \frac{\mathbf{x}_{i+1,j} - \mathbf{x}_{i-1,j}}{2dx} \quad (37a)$$

$$\left(\frac{\partial \mathbf{x}}{\partial y}\right)_{i,j} = \frac{\mathbf{x}_{i,j+1} - \mathbf{x}_{i,j-1}}{2dy} \quad (37b)$$

We use the one-sided upwind differences :

$$\left\{ \begin{array}{l} \left(\frac{\partial \mathbf{x}}{\partial x}\right)_{i,j} = \frac{\mathbf{x}_{i,j} - \mathbf{x}_{i-1,j}}{dx} \text{ if } \mathbf{m}_{i,j}^1 > 0 \\ \left(\frac{\partial \mathbf{x}}{\partial x}\right)_{i,j} = \frac{\mathbf{x}_{i+1,j} - \mathbf{x}_{i,j}}{dx} \text{ if } \mathbf{m}_{i,j}^1 < 0 \end{array} \right. \quad (38a)$$

and

$$\left\{ \begin{array}{l} \left(\frac{\partial \mathbf{x}}{\partial y}\right)_{i,j} = \frac{\mathbf{x}_{i,j} - \mathbf{x}_{i,j-1}}{dy} \text{ if } \mathbf{m}_{i,j}^2 < 0 \\ \left(\frac{\partial \mathbf{x}}{\partial y}\right)_{i,j} = \frac{\mathbf{x}_{i,j+1} - \mathbf{x}_{i,j}}{dy} \text{ if } \mathbf{m}_{i,j}^2 > 0 \end{array} \right. \quad (38b)$$

B.2.2 Third-order upwind scheme (UFDM3)

It can be shown, see e.g. [E. Ewing and Wang, 2001] that the UFDM scheme is actually a second-order approximation of the SPDE with a modified diffusion term. Along this line, it comes with the family of methods that may introduce excessive numerical diffusion in the solution with large gradients. Thus, we use a third order upwind scheme for the approximation of spatial derivatives with four points instead of two, with only a reduced increase in the degree of sparsity of the precision matrix. This scheme is less diffusive compared to the second-order accurate scheme. It comes with four points instead of two for the approximation, with only a reduced increase in the degree of sparsity of the discretized differential operator.

It can be expressed as follows:

$$\left\{ \begin{array}{l} \left(\frac{\partial \mathbf{x}}{\partial x}\right)_{i,j} = \frac{2\mathbf{x}_{i+1,j} + 3\mathbf{x}_{i,j} - 6\mathbf{x}_{i-1,j} + \mathbf{x}_{i-2,j}}{6dx} \text{ if } \mathbf{m}_{i,j}^1 > 0 \\ \left(\frac{\partial \mathbf{x}}{\partial x}\right)_{i,j} = \frac{-\mathbf{x}_{i+2,j} + 6\mathbf{x}_{i+1,j} - 3\mathbf{x}_{i,j} - 2\mathbf{x}_{i-1,j}}{6dx} \text{ if } \mathbf{m}_{i,j}^1 < 0 \end{array} \right. \quad (39a)$$

and

$$\begin{cases} \left(\frac{\partial \mathbf{x}}{\partial y}\right)_{i,j} = \frac{2\mathbf{x}_{i,j+1} + 3\mathbf{x}_{i,j} - 6\mathbf{x}_{i,j-1} + \mathbf{x}_{i,j-2}}{6dy} & \text{if } \mathbf{m}_{i,j}^2 > 0 \\ \left(\frac{\partial \mathbf{x}}{\partial y}\right)_{i,j} = \frac{-\mathbf{x}_{i,j+2} + 6\mathbf{x}_{i,j+1} - 3\mathbf{x}_{i,j} - 2\mathbf{x}_{i,j-1}}{6dy} & \text{if } \mathbf{m}_{i,j}^2 < 0 \end{cases} \quad (39b)$$

B.3 Discretization of the spatio-temporal SPDE

Based on the discretization of the spatial operators using upwind finite difference schemes for the advection term and centered difference schemes for the diffusion term, we involve an implicit Euler scheme to solve the advection-diffusion SPDE:

$$\frac{\partial \mathbf{x}}{\partial t} + \{\kappa^2(\mathbf{s}, t) + \mathbf{m}(\mathbf{s}, t) \cdot \nabla - \nabla \cdot \mathbf{H}(\mathbf{s}, t) \nabla\}^{\alpha/2} \mathbf{x}(\mathbf{s}, t) = \tau(\mathbf{s}, t) \mathbf{z}(\mathbf{s}, t)$$

Because the upwind advection schemes is not symmetric and does not involve the same neighbours in the difference scheme approximation according to the predominant flow direction, we introduce the following generic notations.

$$\begin{cases} \mathbf{m}_{i,j}^{1,t,-} = \left(\frac{\partial \mathbf{x}}{\partial x}\right)_{i,j}^t & \text{if } \mathbf{m}_{i,j}^{1,t} > 0 \\ \mathbf{m}_{i,j}^{1,t,+} = \left(\frac{\partial \mathbf{x}}{\partial x}\right)_{i,j}^t & \text{if } \mathbf{m}_{i,j}^{1,t} < 0 \end{cases} \quad \text{and} \quad \begin{cases} \mathbf{m}_{i,j}^{2,t,-} = \left(\frac{\partial \mathbf{x}}{\partial y}\right)_{i,j}^t & \text{if } \mathbf{m}_{i,j}^{2,t} > 0 \\ \mathbf{m}_{i,j}^{2,t,+} = \left(\frac{\partial \mathbf{x}}{\partial y}\right)_{i,j}^t & \text{if } \mathbf{m}_{i,j}^{2,t} < 0 \end{cases}$$

and by denoting $\mathbf{a}_{i,j}^{1,t,+} = \max(\mathbf{m}_{i,j}^{1,t}, 0)$, $\mathbf{a}_{i,j}^{1,t,-} = \min(\mathbf{m}_{i,j}^{1,t}, 0)$, $\mathbf{a}_{i,j}^{2,t,+} = \max(\mathbf{m}_{i,j}^{2,t}, 0)$, $\mathbf{a}_{i,j}^{2,t,-} = \min(\mathbf{m}_{i,j}^{2,t}, 0)$, the resulting UFD, whatever the order of the scheme, can be written in its compact form as:

$$\begin{aligned} \mathbf{x}_{i,j}^{t+1} = & \mathbf{x}_{i,j}^t + dt \left[\kappa_{i,j}^t \mathbf{x}_{i,j}^t + \left(\mathbf{a}_{i,j}^{1,t,+} \mathbf{m}_{i,j}^{1,t,-} + \mathbf{a}_{i,j}^{1,t,-} \mathbf{m}_{i,j}^{1,t,+} \right) + \left(\mathbf{a}_{i,j}^{2,t,+} \mathbf{m}_{i,j}^{2,t,-} + \mathbf{a}_{i,j}^{2,t,-} \mathbf{m}_{i,j}^{2,t,+} \right) \right. \\ & + \mathbf{H}_{i,j}^{1,1,t} \frac{\mathbf{x}_{i+1,j}^t - 2\mathbf{x}_{i,j}^t + \mathbf{x}_{i-1,j}^t}{dx^2} + \mathbf{H}_{i,j}^{2,2,t} \frac{\mathbf{x}_{i,j+1}^t - 2\mathbf{x}_{i,j}^t + \mathbf{x}_{i,j-1}^t}{dy^2} \\ & \left. + \mathbf{H}_{i,j}^{1,2,t} \frac{\mathbf{x}_{i+1,j+1}^t - \mathbf{x}_{i+1,j-1}^t - \mathbf{x}_{i-1,j+1}^t + \mathbf{x}_{i-1,j-1}^t}{2dxdy} + \tau_{i,j}^t \mathbf{z}_{i,j} \right] \end{aligned}$$

Using again notation $i = \lfloor k/N_x \rfloor$ and $j = k \bmod N_x$, operator \mathbf{A}_t associated to UFD, finally writes:

$$\mathbf{A}_{k,l}(t) = \begin{cases} \mathbf{H}_{i,j}^{1,2,t} / 2dxdy & \text{if } l = k \pm (N_x + 1) \\ \mathbf{H}_{i,j}^{1,2,t} / 2dxdy & \text{if } l = k \pm (N_x - 1) \\ -\mathbf{H}_{i,j}^{1,1,t} / dx^2 + \left(\mathbf{a}_{i,j}^{1,t,+} + \mathbf{a}_{i,j}^{1,t,-} \right) / dx & \text{if } l = k - 1 \\ -\mathbf{H}_{i,j}^{1,1,t} / dx^2 + \left(\mathbf{a}_{i,j}^{1,t,+} + \mathbf{a}_{i,j}^{1,t,-} \right) / dx & \text{if } l = k + 1 \\ -\mathbf{H}_{i,j}^{2,2,t} / dy^2 + \left(\mathbf{a}_{i,j}^{2,t,+} + \mathbf{a}_{i,j}^{2,t,-} \right) / dy & \text{if } l = k - N_x \\ -\mathbf{H}_{i,j}^{2,2,t} / dy^2 + \left(\mathbf{a}_{i,j}^{2,t,+} + \mathbf{a}_{i,j}^{2,t,-} \right) / dy & \text{if } l = k + N_x \\ \left(\kappa_{i,j}^t \right)^2 + 2(\mathbf{H}_{i,j}^{1,1,t} / dx^2 + \mathbf{H}_{i,j}^{2,2,t} / dy^2) \\ + \left(\mathbf{a}_{i,j}^{1,t,+} + \mathbf{a}_{i,j}^{1,t,-} \right) / dx + \left(\mathbf{a}_{i,j}^{2,t,+} + \mathbf{a}_{i,j}^{2,t,-} \right) / dy & \text{if } k = l \\ 0 & \text{otherwise} \end{cases} \quad (40)$$

The same operator associated to UFD3M writes:

$$\mathbf{A}_{k,l}(t) = \begin{cases} \mathbf{H}_{i,j}^{1,2,t} / 2dx dy & \text{if } l = k \pm (N_x + 1) \\ \mathbf{H}_{i,j}^{1,2,t} / 2dx dy & \text{if } l = k \pm (N_x - 1) \\ \mathbf{a}_{i,j}^{1,t,+} / 6dx & \text{if } l = k - 2 \\ -\mathbf{H}_{i,j}^{1,1,t} / dx^2 - \left(6\mathbf{a}_{i,j}^{1,t,+} + 2\mathbf{a}_{i,j}^{1,t,-} \right) / 6dx & \text{if } l = k - 1 \\ -\mathbf{H}_{i,j}^{1,1,t} / dx^2 + \left(2\mathbf{a}_{i,j}^{1,t,+} + 6\mathbf{a}_{i,j}^{1,t,-} \right) / 6dx & \text{if } l = k + 1 \\ -\mathbf{a}_{i,j}^{1,t,-} / 6dx & \text{if } l = k + 2 \\ \mathbf{a}_{i,j}^{2,t,+} / 6dy & \text{if } l = k - 2N_x \\ -\mathbf{H}_{i,j}^{2,2,t} / dy^2 - \left(6\mathbf{a}_{i,j}^{2,t,+} + 2\mathbf{a}_{i,j}^{2,t,-} \right) / 6dy & \text{if } l = k - N_x \\ -\mathbf{H}_{i,j}^{2,2,t} / dy^2 + \left(2\mathbf{a}_{i,j}^{2,t,+} + 6\mathbf{a}_{i,j}^{2,t,-} \right) / 6dy & \text{if } l = k + N_x \\ -\mathbf{a}_{i,j}^{2,t,-} / 6dy & \text{if } l = k + 2N_x \\ \left(\kappa_{i,j}^t \right)^2 + 2\left(\mathbf{H}_{i,j}^{1,1,t} / dx^2 + \mathbf{H}_{i,j}^{2,2,t} / dy^2 \right) \\ + 3 \left(\mathbf{a}_{i,j}^{1,t,+} - \mathbf{a}_{i,j}^{1,t,-} \right) / 6dx \\ + 3 \left(\mathbf{a}_{i,j}^{2,t,+} - \mathbf{a}_{i,j}^{2,t,-} \right) / 6dy & \text{if } k = l \end{cases} \quad (41)$$

and 0 otherwise.

C PyTorch implementation of sparse linear algebra

Currently, two pieces of codes are missing in the PyTorch sparse linear algebra to achieve a fully sparse implementation of our algorithm: the automatic differentiation tools for

- solving sparse linear systems
- running sparse Cholesky decomposition

First, regarding the implementation of the backward pass for solving linear systems, we start by writing the forward pass of this system of equation:

$$x = \mathbf{A}^{-1}\mathbf{b}$$

where \mathbf{A} denotes a $2D$ square matrix and \mathbf{b} a one-dimensional vector.

We need to provide the gradients wrt both \mathbf{A} and \mathbf{b} :

$$\begin{aligned} \frac{\partial L}{\partial \mathbf{b}} &= \frac{\partial L}{\partial x_i} \frac{\partial x_i}{\partial \mathbf{b}_j} = \frac{\partial L}{\partial x_i} \frac{\partial}{\partial \mathbf{b}_k} (\mathbf{A}_{ij}^{-1} \mathbf{b}_j) = \frac{\partial L}{\partial x_i} \mathbf{A}_{ij}^{-1} \frac{\partial \mathbf{b}_j}{\partial \mathbf{b}_k} \\ &= \frac{\partial L}{\partial x_i} \mathbf{A}_{ij}^{-1} \delta_{jk} = \frac{\partial L}{\partial x_i} \mathbf{A}_{ik}^{-1} = (\mathbf{A}^{-1})^T \frac{\partial L}{\partial x} \\ &= \text{solve}(\mathbf{A}^T, \frac{\partial L}{\partial x}) \end{aligned}$$

and

$$\begin{aligned} \frac{\partial L}{\partial \mathbf{A}} &= \frac{\partial L}{\partial x_i} \frac{\partial x_i}{\partial \mathbf{A}_{mn}} = \frac{\partial L}{\partial x_i} \frac{\partial}{\partial \mathbf{A}_{mn}} (\mathbf{A}_{ij}^{-1} \mathbf{b}_j) \\ &= -\frac{\partial L}{\partial x_i} \mathbf{A}_{ij}^{-1} \frac{\partial \mathbf{A}_{jk}}{\partial \mathbf{A}_{mn}} \mathbf{A}_{kl}^{-1} \mathbf{b}_l \\ &= -\frac{\partial L}{\partial x_i} \mathbf{A}_{ij}^{-1} \delta_{jm} \delta_{kn} \mathbf{A}_{kl}^{-1} \mathbf{b}_l \\ &= -\frac{\partial L}{\partial x_i} \mathbf{A}_{im}^{-1} \mathbf{A}_{nl}^{-1} \mathbf{b}_l \\ &= -\left((\mathbf{A}^{-1})^T \frac{\partial L}{\partial x} \right) \otimes (\mathbf{A}^{-1} \mathbf{b}) \\ &= -\frac{\partial L}{\partial \mathbf{b}} \otimes x \end{aligned}$$

where we used the einstein summation convention during the derivations, as well as the following identity:

$$\frac{\partial (\mathbf{A}^{-1})}{\partial p} = -\mathbf{A}^{-1} \frac{\partial \mathbf{A}}{\partial p} \mathbf{A}^{-1}.$$

These two expressions $\frac{\partial L}{\partial \mathbf{b}}$ and $\frac{\partial L}{\partial \mathbf{A}}$ are easily implemented in PyTorch based on sparse representations.

Second, the backward pass for a sparse Cholesky decomposition may be found for instance in Seeger et al. [2019]: given a symmetric, positive definite matrix \mathbf{A} , its Cholesky factor \mathbf{L} is lower triangular with positive diagonal, such that the forward pass of the Cholesky decomposition is defined as $\mathbf{A} = \mathbf{L}\mathbf{L}^T$. Given the output gradient $\bar{\mathbf{L}}$ and the Cholesky factor \mathbf{L} , the backward pass compute the input gradient $\bar{\mathbf{A}}$ defined as :

$$\bar{\mathbf{A}} = \frac{1}{2} \mathbf{L}^{-T} \text{ltu}(\mathbf{L}^T \bar{\mathbf{L}}) \mathbf{L}^{-1} \quad (42)$$

where $\text{ltu}(\mathbf{X})$ generates a symmetric matrix by copying the lower triangle to the upper triangle. In our work, such an operation is useful when optimizing the likelihood in the outer training cost function of the neural scheme, see Eq. 28, which involves the determinant of sparse matrices Cholesky decomposition.

D QG-based analysis

Coming back to the validation and interpretability of the proposed framework, we can also draw from the simplified one-layer quasi-geostrophic (QG) to propose an additional SPDE formulation. In the QG theory, see e.g. [Ubelmann et al., 2014], which is acceptable over this Gulf Stream domain, we assume that potential vorticity $q(\mathbf{s}, t)$ defined as:

$$\mathbf{q}(\mathbf{s}, t) = \frac{g}{f} \left(\Delta - \frac{1}{L_r^2} \right) \mathbf{x}(\mathbf{s}, t) \quad (43)$$

where \mathbf{x} still denotes the SSH, g is the gravity constant, f is the Coriolis parameter and L_R is the first Rossby deformation radius, is advected by the geostrophic velocities (\mathbf{m}_g):

$$\frac{\partial q}{\partial t} + \mathbf{m}_g \cdot \nabla = 0 \quad (44)$$

In this application, especially in the context of the upcoming wide-swath SWOT datasets, see e.g. Metref et al. [2020], on which the potential vorticity can be directly computed based on the numerical discretization of Eq. (43):

$$\mathbf{q} = \mathbf{A}\mathbf{x}$$

with $\mathbf{A} = \text{FDM} \left(\frac{g}{f} \left(\Delta - \frac{1}{L_r^2} \right) \right)$, future works may be to propose a surrogate SPDE model with single advection terms as a stochastic QG parametrization of the potential vorticity.

The proposed framework will be applied on the latter instead of working on the raw SSH. In the end, the final SSH reconstruction would be obtained by:

$$\mathbf{x} = \mathbf{A}^{-1} \mathbf{q}^*$$